HIGH T-LOW P METAMORPHISM IN THE KANAPPA HILL AREA OF THE MOUNT LOFTY RANGES, S.A.; IMPLICATIONS FOR THERMAL EVOLUTION

GEOFFREY L. FRASER

Submitted as partial fulfilment of the degree of B.Sc.(Hons) in the Department of Geology and Geophysics at the University of Adelaide, Nov. 1990.

TABLE OF CONTENTS

List of Figures

Plates

Tables

ABSTRACT

High T - low P metamorphic rocks in the Kanappa Hill area of the eastern Mt. Lofty Ranges preserve evidence for mineral equilibration during crustal thickening at temperatures marginally greater than 600°C and pressures of 3-5 kbars. Field and petrographic observations suggest that the high temperature portion of the P-T-t path experienced by these rocks was near-isobaric, with the implication that the thermal perturbation recorded by these rocks occurred in response to rapid advective heat transfer rather than to purely conductive processes. Estimation of the metamorphic fluid flux from a stable isotope study indicates that pervasive fluid flushing made no significant contribution to the thermal perturbation. Thermomechanical modelling of the response of the crust to magma emplacement predicts metamorphic conditions which closely match observations from the field, viz: (1) peak metamorphic temperatures reached during convergent orogenesis, (2) near isobaric P-T-t paths immediately before and after attainment of peak metamorphic conditions. Consequently high T - low P metamorphism in the Kanappa Hill Area is considered to have occurred in response to upper crustal emplacement of melts generated by subcrustal heat input.

1. INTRODUCTION

Much of the interest in metamorphic rocks stems from their ability to record the effects of orogenic processes, particularly perturbations to the steady state thermal regime of continental crust. In this context the steady state continental geotherm provides a theoretical yardstick with which specific terrains may be compared and classified. One such class of metamorphic terrains, the "Buchan Style" terrains, named after their type area in Scotland, is characterised by high temperature (T) - low pressure (P) mineral assemblages. These High T - Low P "Buchan Style" metamorphic terrains frequently preserve evidence for mineral equilibration at temperatures in excess of 600°C and depths less than 15km (4-5kbars) and thus record a substantial high temperature perturbation to the steady state crustal geotherm (Fig. 1). High temperature perturbation of the thermal regime during orogenesis may theoretically be controlled by three major factors; (1) deformation; (2) magma input, and (3) metamorphic fluid flow. Consequently any understanding of the thermal evolution of a specific terrain involves evaluating the relative contribution of each of these processes.

Previous investigations in the Eastern Mount Lofty Ranges have shown that this area is a clear example of a "Buchan Style" terrain (Mills, 1964; Offler and Fleming, 1968; Abbas, 1972; Mancktelow, 1979; Sandiford et.al., 1990). However, apart from some preliminary calculations provided by Sandiford et.al. (1990), a detailed understanding of the thermal processes contributing to the formation of this terrain is still lacking, particularly with respect to the mode of heat transfer into the orogen. The present study addresses this problem using evidence gained from detailed field and laboratory investigation of the metamorphic rocks in the Kanappa Hill area combined with theoretical considerations and numerical modelling. Specifically this study attempts to determine the likely cause for the thermal perturbation in the Kanappa Hill region by considering each of the three theoretically plausible causes mentioned above and comparing their predicted effects with observations made in the field and in the laboratory.

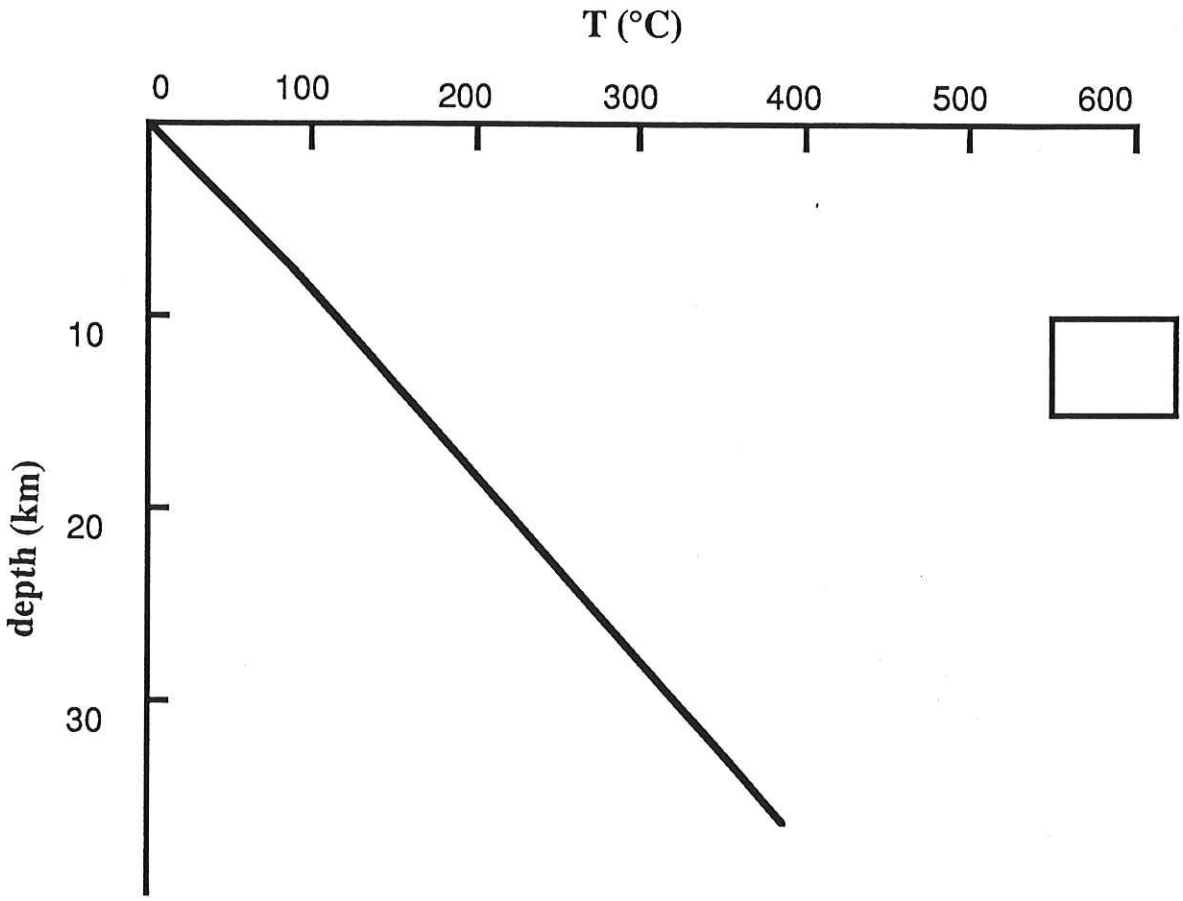

Figure 1 A typical, steady state, continental geotherm with the P-T conditions recorded by rocks in the Kanappa Hill area indicated by the box. The geotherm is calculated via the equation

$$T = T_S + \frac{q_m\, y}{k} + \frac{(q_s - q_m)\, h_r}{k}(1 - e^{-y/h_r})$$

where the symbols and their assumed values are;
T_S is the surface temperature (10°C), qm is the heat flow through the base of the crust (30mWm-2), qs is the heat flow through the earth's surface (56.5mWm-2), y is depth, k is the coefficient of thermal conductivity (3.35Wm-1°K-1), hr is a length scale for the decay of heat prodcing elements in the crust (10km).

Kanappa Hill is situated approximately 15 km east of Springton, in an area bounded on the eastern side by the Tertiary fault scarp of the Murray Plains, and lying within the amphibolite grade zone of Mills (1964) (Fig. 2). Detailed mapping of mineral assemblages and their relation to structural fabrics has been carried out in order to establish constraints on the variation of pressure (P), temperature (T) and timing (t) of metamorphism across the area. The mapped area is a southerly extension of the area discussed by Arnold (1989), giving a combined transect of ~12 km obliquely up metamorphic grade. Lines of evidence used include;

(1) timing of mineral growth with respect to structural fabrics, which gives an indication of the relation between deformation and metamorphism:

(2) recognition of systematic changes in the mineral assemblages observed across this transect, which show the gradient in peak metamorphic conditions across the area:

(3) identification of retrograde and relict prograde assemblages, which provide constraints on the form of the P-T-t paths experienced by these rocks:

(4) a stable isotope study across a marble band, which provides an estimation of the total metamorphic fluid flux through the terrain:

(5) a numerical model which simulates the thermal evolution of the crust following magma input which allows a comparison of predicted effects of intrusion with observations from the Kanappa Hill area.

2. GEOLOGY OF THE KANAPPA HILL AREA

2.1. Geological Background

The Mt Lofty Ranges form part of the Adelaide Fold Belt, an arcuate belt of late Proterozoic to early Palaeozoic sedimentary rocks which were deformed and metamorphosed during the Cambro-Ordovician Delamerian Orogeny. Through most of the fold belt the

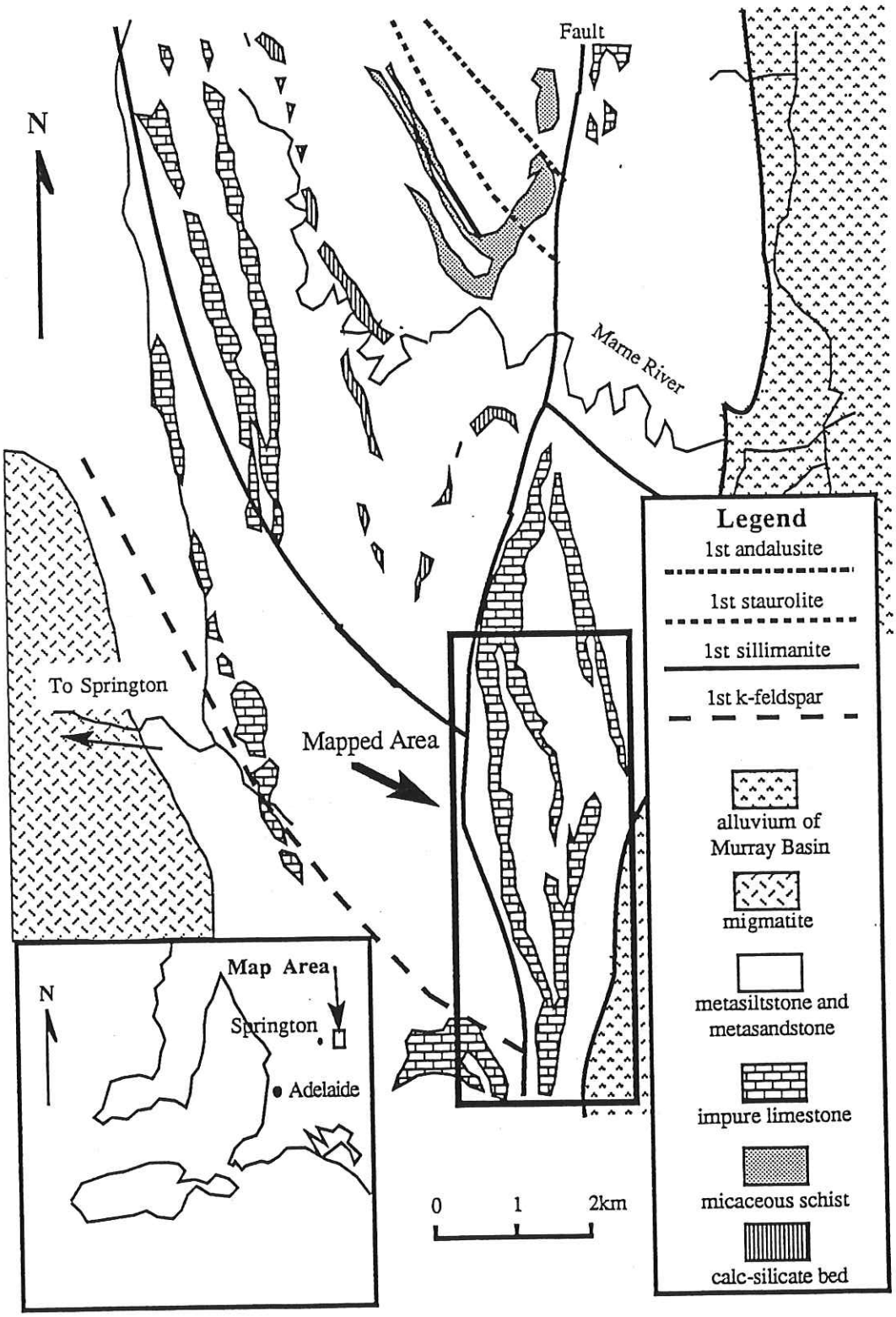
Fault
N
Marne River
To Springton
Mapped Area
Map Area
N
Springton
Adelaide
0
1
2km
Legend
1st andalusite
1st staurolite
1st sillimanite
1st k-feldspar
alluvium of Murray Basin
migmatite
metasiltstone and metasandstone
impure limestone
micaceous schist
calc-silicate bed

metamorphic grade is very low; however in the Eastern Mt Lofty Ranges the sediments have locally been subjected to high grade metamorphism. The highest grade rocks are concentrated in a roughly north-south trending band centred around outcrops of felsic intrusives between Palmer and the Barossa Valley e.g. Rathjen Gneiss, Reedy Creek Granodiorite, with grade decreasing progressively with distance from these intrusives. Kanappa Hill is located approximately 5km NNE of this band of intrusives.

2.2. Kanappa Hill Region

Detailed descriptions of lithologies and comprehensive structural studies of the region can be found elsewhere (Mills, 1964; Fleming, 1971; Mancktelow, 1979). Consequently what is presented here is a simple overview of the geology and structure seen in the mapped area, concentrating on its implications for metamorphic and thermal evolution.

Morphologically the mapped area provides a striking contrast between the steep hills and deeply cut creeks west of a Tertiary fault scarp and the Quaternary sediment-covered Murray Plains to the east. The Palaeozoic sequence here constitutes part of the Blowhole Creek Member of the basal Carrickalinga Head Formation of the Kanmantoo Group, the rocks being predominantly quartz-biotite schists with the distinctive Millendella Marble horizon providing a useful stratigraphic marker bed (Cooper, 1989). A massive quartz-albite unit forms Kanappa Hill, the highest point in the area.

2.3. Structure

In accordance with previous work (Offler and Fleming, 1968) three phases of ductile deformation are recognized. The dominant structural fabric in the region is a steeply dipping schistosity best defined in micaceous schists and axial planar to upright to slightly reclined, tight to isoclinal folds. These folds are seen on the mesoscopic scale throughout the area and are considered responsible for the macroscopic outcrop pattern (Fig. 11). Fold style varies with lithology, being angular in marble and more rounded in the schists but is asymmetric throughout with axial planes steeply dipping (Plate 1a). Although these tight to isoclinal folds

a

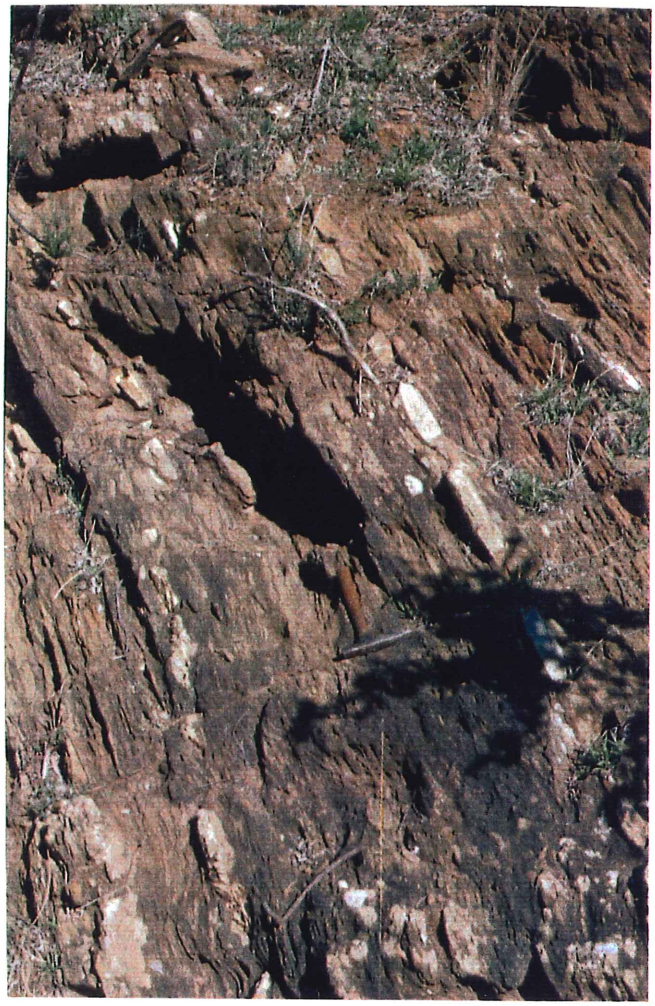

b

c

mean that over much of the area the axial planar fabric is parallel to compositional variations, they are sometimes seen to crenulate biotite-rich laminae implying the existence of an earlier fabric (Plate 2a). Hence the upright folds and associated fabric are considered to be a product of the second deformation (D_2) and are here referred to as F_2 and S_2. Orientation of the S_2 axial planar fabric is NNW and the plunge of the F_2 axes is variable from 30° north to 30° south.

The preceding deformation (D_1) is recognized largely due to the existence of crenulation cleavage development in F_2 folds with only one outcrop showing folding on a mesoscopic scale attributable to F_1. In this outcrop the F_1 folding is almost flat- lying and isoclinal in a finely laminated schist with the axial trace oriented slightly more westerly than F_2. Allen (1977) also recognized a deformation predating the dominant regional schistosity through the observation of an internal fabric in porphyroblasts discontinuous with S_2. The flat lying nature of the F_1 folds is consistent with observations made by Martin (1990) of early, flat lying fabrics around the Rathjen Gneiss, several kilometres south of Kanappa Hill.

Two phases of felsic intrusion are recognized in some outcrops, both predating D_2 with veins either exhibiting F_2 style folding or else boudinaged in the S_2 plane (Plate 1c). Leucocratic veins and quartz segregations strung out in the foliation plane indicate a substantial vertical component of extensional strain during D_2 (i.e. subvertical principal stretching direction) suggesting that this deformation was responsible for bulk crustal thickening (Plate 1b).

A third phase of ductile deformation is recognized only on the eastern side of the area, south of Kanappa Creek where S_2 has been folded on a scale of 100m. F_3 is unequivocally later than S_2 and distinctly different in orientation to F1 and F_2, suggestive of a significant change in the stress field post dating the major deformational event.

Evidence of brittle thrusting post dating D_2 can be seen in several outcrops with the implied thrusting direction always being west to east. This contrasts with most regional interpretations for the Adelaide Fold Belt (Jenkins,1990) in which thrusting is invoked from

east to west. The multiple west to east thrusts seen in the field are small scale and may be the result of backthrusting in association with more major east- west thrusts (Butler, 1982). Indeed Mills (1964) and others (Abbas, 1972; Mancktelow, 1979) have interpreted one of these major thrusts to run down the western margin of the mapped area although the only field evidence found to support this was a crush zone in a road cutting 1km south of the area. The major thrusting in the Adelaide Fold Belt as mapped by Mills (1964), Abbas (1972) and Mancktelow (1979) displaces metamorphic isograds and therefore post dates metamorphism.

Finally, Tertiary uplift of the Adelaide Hills has produced steeply dipping breccia zones in schists along the fault scarp defining the Murray Plains along the east of the mapped area. These breccia zones are responsible for some disruption in orientation of earlier fabrics.

In summary the field relations reveal three distinct phases of ductile deformation, D_2 being the most pervasive and suggestive of significant crustal thickening in response to east west shortening.

2.4. Metamorphism

Regional mapping of mineral assemblages in the Mt Lofty Ranges (Offler and Fleming, 1968) has shown a concentric zoning of metamorphic grade around a roughly NW-SE band of intrusives including the Rathjen Gneiss, Palmer Granite and Reedy Creek Granodiorite. This evidence points to these intrusions as being at least partly responsible for the metamorphism. The Kanappa Hill area is situated up-grade of the sillimanite-K feldspar isograd with the mapped area forming an oblique section across the isograds as mapped by Mills (1964). In this area metamorphic grade increases systematically towards the SW-SSW. The dominant rock type in the area, as through much of the Kanmantoo Group, is a biotite, quartz, plagioclase semi-pelite. This high variance assemblage provides no useful constraints on P-T-X_{fluid} conditions during metamorphism. However three distinct lithological associations containing diagnostic metamorphic mineral assemblages do occur within the mapped area, namely; pelitic schists, potassium-depleted orthoamphibole rocks and marbles. Each of these rock types will be discussed in turn with regard to their assemblages and their

implications for metamorphic history. The characteristic mineral assemblages in each group are summarised in Table 2.

2.4.1. Pelitic Schists

Pelitic schists are widespread in the study area (Fig.11) and characteristically contain the prograde assemblage quartz, biotite, albite, sillimanite and K-feldspar. Sillimanite occurs as fibrous aggregates growing in the S_2 foliation plane defined by alignment of biotite grains (Plate 2b). Though andalusite is not seen, the aggregated habit of sillimanite is suggestive of its growth being due to the breakdown of andalusite as has been documented 2km to the north (Arnold and Sandiford,1990) and approximately 7km to the NW at the Marne Reserve (Sandiford et.al., 1990) where kyanite is also preserved. In sample 933-52 garnet occurs in a sillimanite-bearing pelite. In addition this rock contains a retrograde st-chl-mu assemblage (Plate 2 e,f).

Aluminosilicate phase relationships from pelitic schists place important constraints on the nature of the prograde P-T path. The occurrence of sillimanite immediately indicates that these rocks have experienced high T and relatively low P metamorphism. The existence of relict early kyanite and subsequent replacement firstly by andalusite and then sillimanite requires a prograde P-T path passing through all three aluminosilicate polymorph stability fields, constraining the path to pressures less than the aluminosilicate triple point. Such a path necessarily involves substantial heating without appreciable accompanying decompression, an important point when considering mechanisms responsible for the metamorphism. Prograde andalusite occurs with sillimanite approximately 2 km down grade of the mapped area (Arnold and Sandiford, in press) north of Kanappa Hill suggesting that the maximum temperatures reached here lay on or close to the andalusite-sillimanite transition. In contrast, the absence of relict prograde andalusite in the mapped area suggests that here temperatures reached well into the sillimanite field. Sillimanite growing with a preferred orientation in the S_2 plane implies high temperatures were reached coeval with the D_2 crustal thickening event in the Kanappa Hill area. A T-X_{Fe} section in the KFMASH system, constructed for pressure of 4.5 kbars

TABLE 1

Mineral abbreviations used in text and figures

bt	biotite	**st**	staurolite
cd	cordierite	**chl**	chlorite
gt	garnet	**mu**	muscovite
gd	gedrite	**and**	andalusite

TABLE 2

Assemblages seen in pelitic schists, orthoamphibole bearing schists and marbles
P = prograde, R = retrograde, p = porphyroblastic, b = after biotite, k = rimmed by cordierite

	933-52	933-30	933-45	933-53	933-54	890-134	890-135
Biotite	P	P	P	P	P	P	P
Plagioclase	P	P	P	P	P	P	P
K-feldspar	P				P		
Quartz	P	P	P	P	P	P	P
Garnet	P	P		P	P		P
Cordierite		Pp			Pp		
Gedrite		P	P	P			P
Sillimanite	P						
Staurolite	R	Pk					
Chlorite	Rb					Rb	
Muscovite	R	R					

	933-55	933-23	933-24
Garnet		P	
Diopside	P	P	P
Epidote	P		P
Actinolite			P
Calcite	P	P	P
Vesuvianite		P	P

a

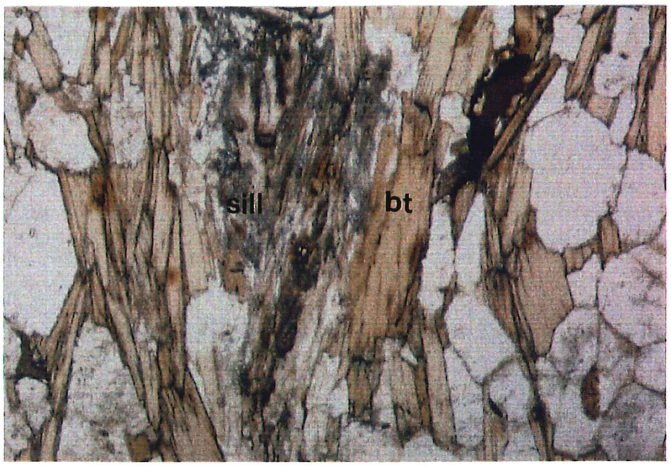

b

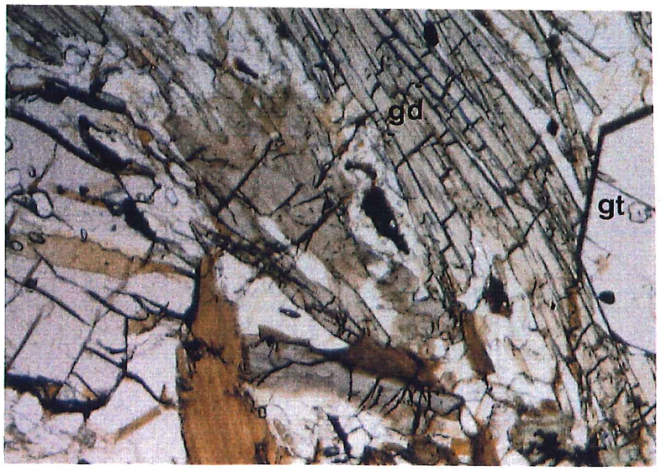

c

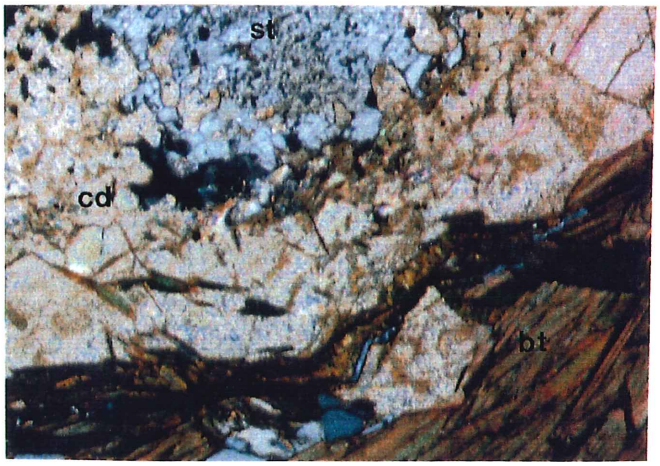

d

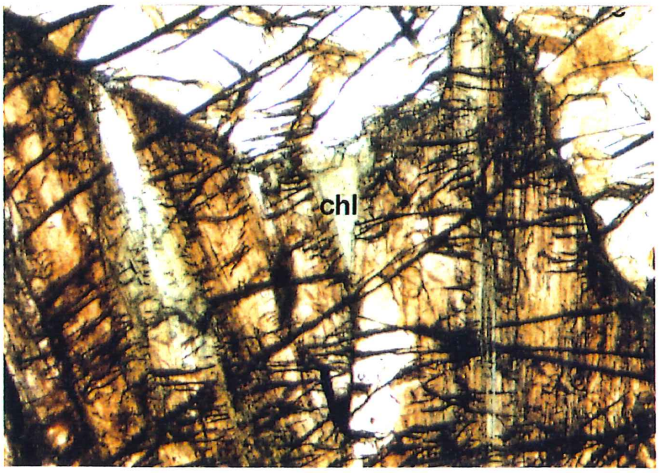

e

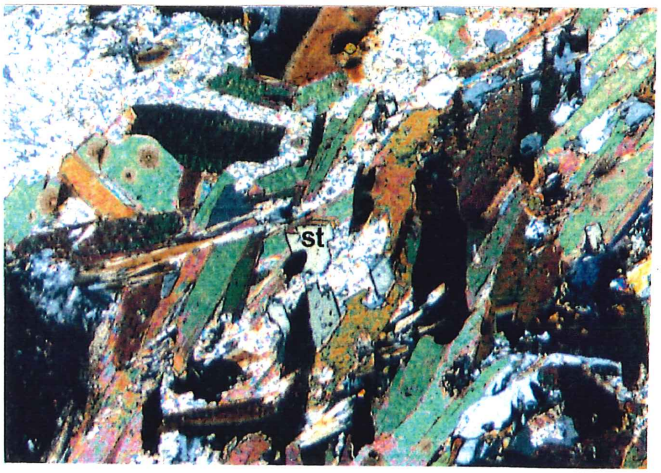

f

(as estimated by Sandiford et. al., 1990) shows that the coexistence of garnet and sillimanite requires temperatures of at least 610°C (Fig. 3). Garnet-biotite geothermometry on the garnet-silllimanite bearing rock (933-52), using the calibration of Ferry and Spear (1978) yields a slightly higher temperature prediction of 631°C. The retrograde st-chl assemblage in sample 933-52 constrains the nature of the P-T cooling path. For pressures of 3kbars a temperature estimate of 570°C, or lower for higher pressures, is derived using the program THERMOCALC (Powell and Holland, 1988). A KFMASH P-T pseudo section for an X_{Fe} appropriate to the bulk rock, in this case ~0.8, shows a minimum pressure for the st-chl assemblage of 3kbars (Fig. 4). The presence of st+chl but not cd+chl or cd+and is suggestive of pressures closer to 4kbars or greater for this section of the retrograde P-T-t path. This is strong evidence against significant (ie. >1.5 kbars) decompression during cooling and is suggestive of a cooling history which was relatively isobaric or possibly involved some further compression.

2.4.2. Orthoamphibole Rocks

Orthoamphibole-bearing rocks occur throughout the mapped area but are confined in scattered pods, with dimensions of tens of metres, rather than being continuous along strike. In these rocks gedrite occurs in association with cordierite or garnet (Plate 2c) or both as well as quartz, albite and biotite. Staurolite, where present, is not in equilibrium relations but is rimmed by cordierite (Plate 2d). This accords with observations down grade where cordierite-gedrite assemblages are considered a result of the breakdown of biotite and staurolite or andalusite accompanied by metasomatic depletion of potassium (Arnold and Sandiford, 1990).

The following progression of mineral associations with orthoamphibole is recognized from north to south; gd+st+cd--> gd+cd-->gd+cd+gt--> gd+gt. Such a progression can be understood by considering the stability of these minerals for a specific composition in the FMASH system and reflects a progressive, and closely isobaric increase in peak temperature from north to south (Fig. 5). A T-X_{Fe} section in the FMASH system, appropriate for the

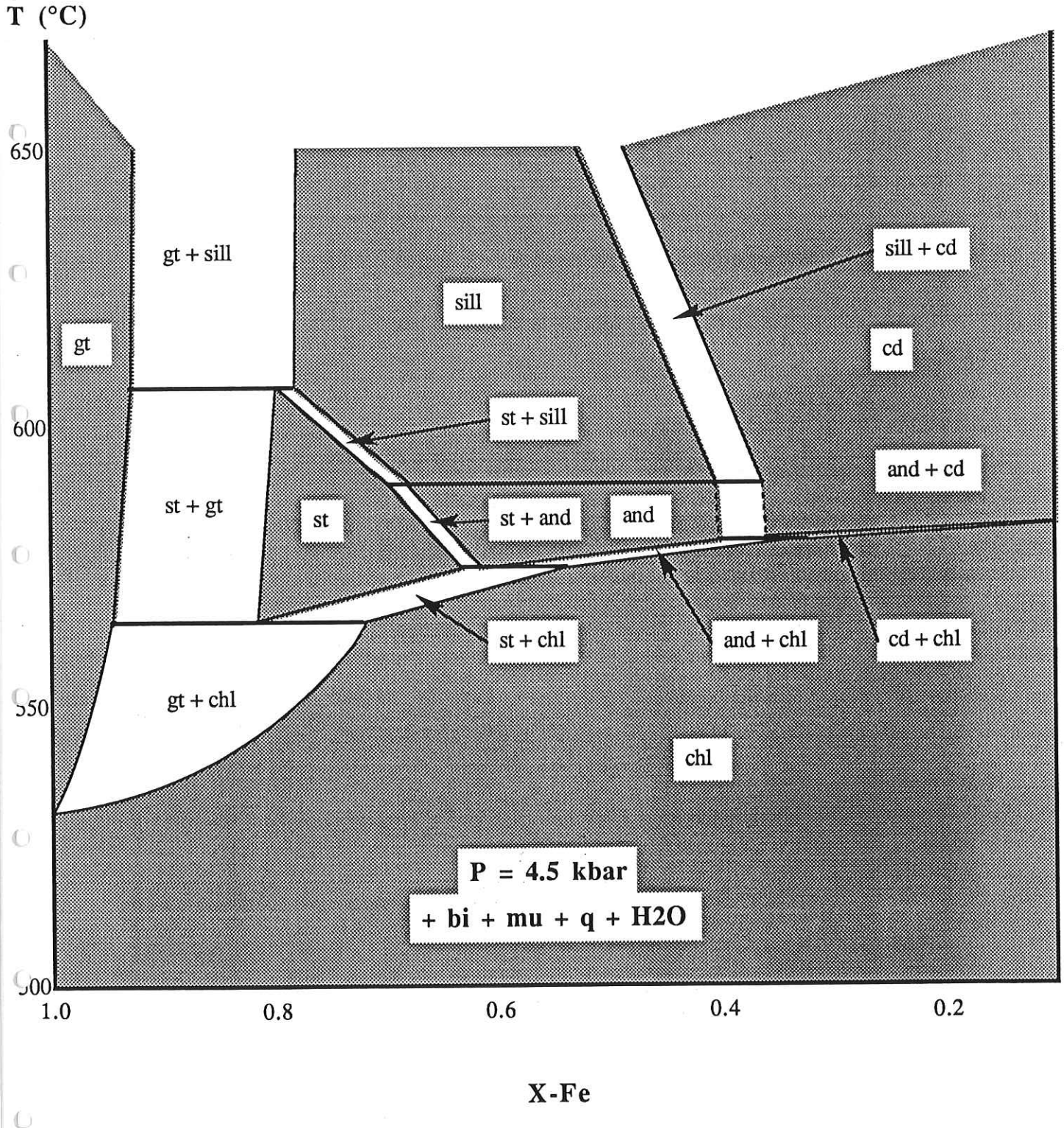

Figure 3 T-XFe section in the KFMASH system, constructed for pressure of 4.5 kbars illustrating temperatures of > 610°C are required for gt-sill stability.(from Dymoke and Sandiford, submitted)

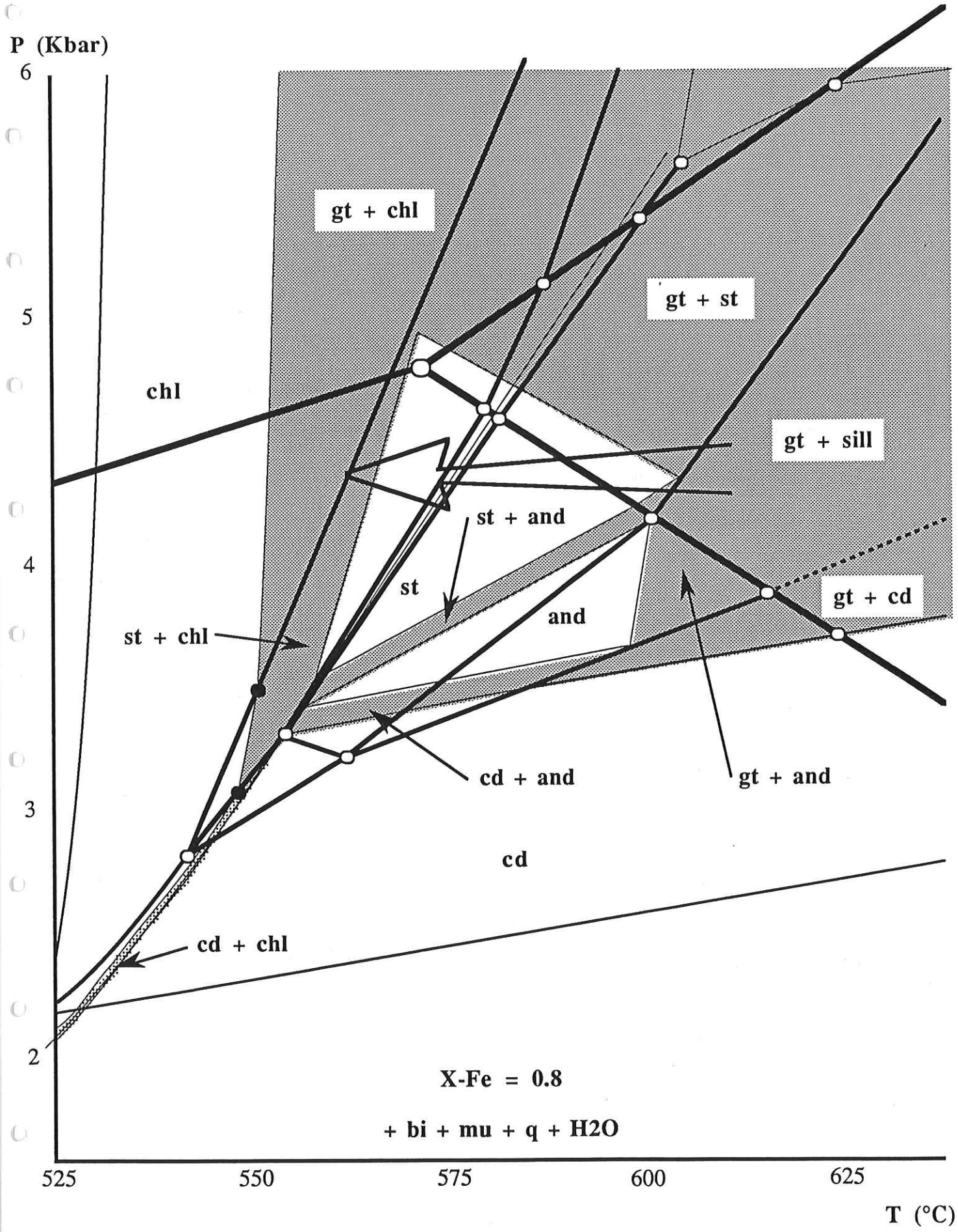
P (Kbar)
6
5
4
3
2
gt + chl
gt + st
gt + sill
gt + cd
chl
st + and
st
and
st + chl
cd + and
gt + and
cd
cd + chl
X-Fe = 0.8
+ bi + mu + q + H2O
525
550
575
600
625
T (°C)

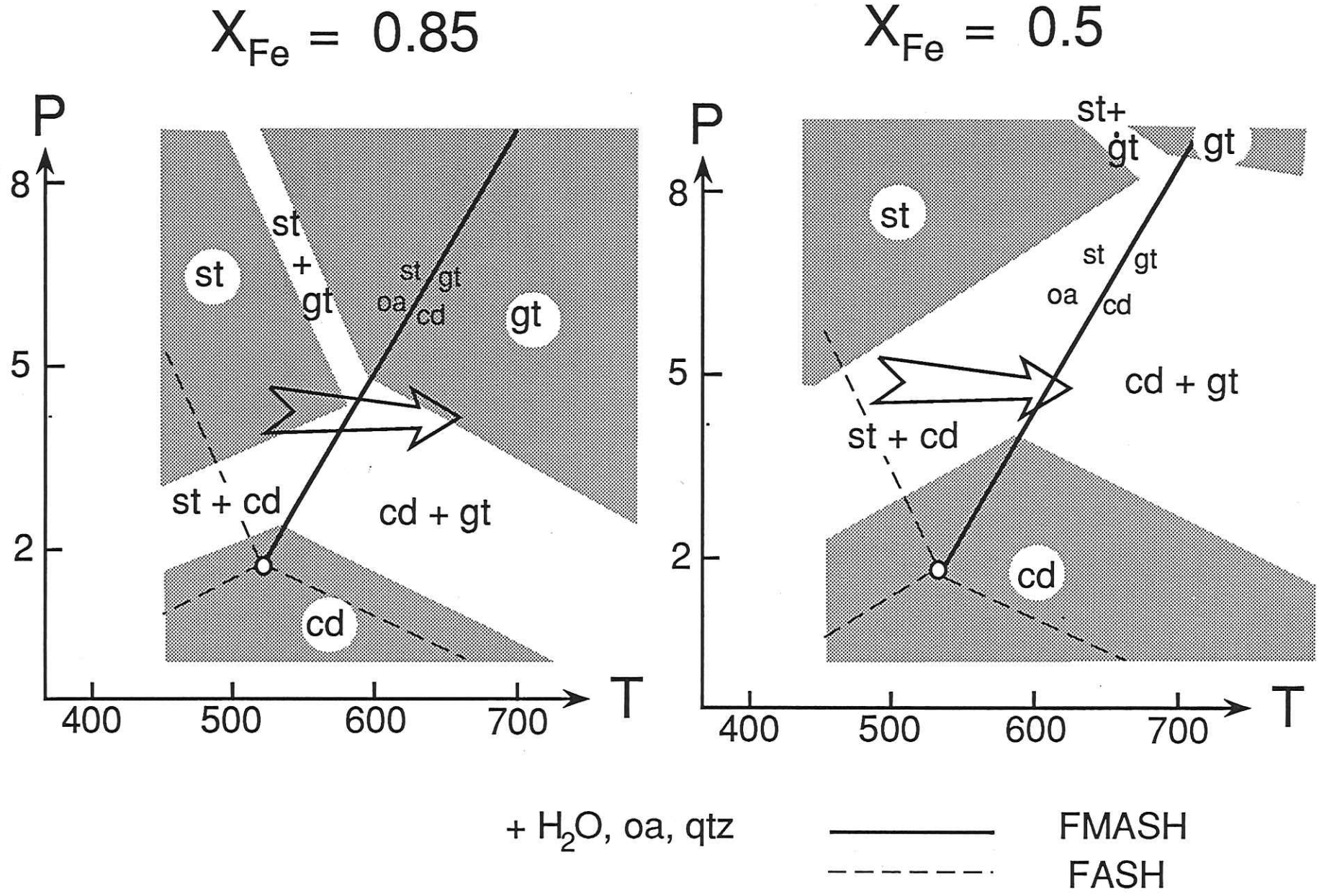
X_{Fe} = 0.85
X_{Fe} = 0.5
P
T
8
5
2
400
500
600
700
st
gt
cd
st + gt
st + cd
cd + gt
oa
st+ gt
+ H2O, oa, qtz
FMASH
FASH

orthoamphibole-bearing rocks, can be used in conjunction with detailed mineral compositional data to generate quantitatively the metamorphic field gradient. Such a section has been constructed using data from THERMOCALC (Powell and Holland, 1988). X_{Fe} values for coexisting garnet and cordierite in sample A933-54 indicate that the stability fields must be displaced towards more iron rich values to be appropriate for rocks from the Kanappa Hill region. The reason for this innaccuracy in the theoretically-constructed section is likely to come from a combination of assumed ideal mixing between iron and magnesium end members and the presence of additional components to FMASH, particularly in garnet. However the general form of the calculated section will still be valid and is retained while the positions of the curves have been adjusted to fit the observed mineral compositions (Fig. 6). X_{Fe} data for coexisting staurolite and cordierite (sample A911-48) then give an indication of temperature of their equilibration, ~580°C.

The first appearance of garnet-cordierite assemblages (sample 933-30) occurs 3km south of the lower T st-cd assemblage and from the section must have equilibrated at at least 600°C. This distance of three kilometres is measured at ~45° to the isograds. Correction for this angle gives a peak temperature gradient of ~11-12°C/km in this region of the terrain. Further north, near the Marne River, gradients have been calculated at 8-10°C/km (Peter Dymoke, pers. comm.) It would appear that gradient of peak temperature with distance steepens up grade, an important observation when considering the nature of the heat source as will be discussed later.

Since it has been shown (Arnold and Sandiford,1990) that the stability of the orthoamphibole-cordierite assemblages is dependent on metasomatic depletion of potassium, the distribution of these assemblages is therefore considered to reflect the geometry of fluid flow through the terrain. The pod-like distribution of these rocks, and petrological evidence for internal buffering of the activity of water in adjacent pelites (Arnold and Sandiford,1990) suggests non-pervasive, channelled flow. The geometry and scale of fluid flow are discussed further in Section 3.1.

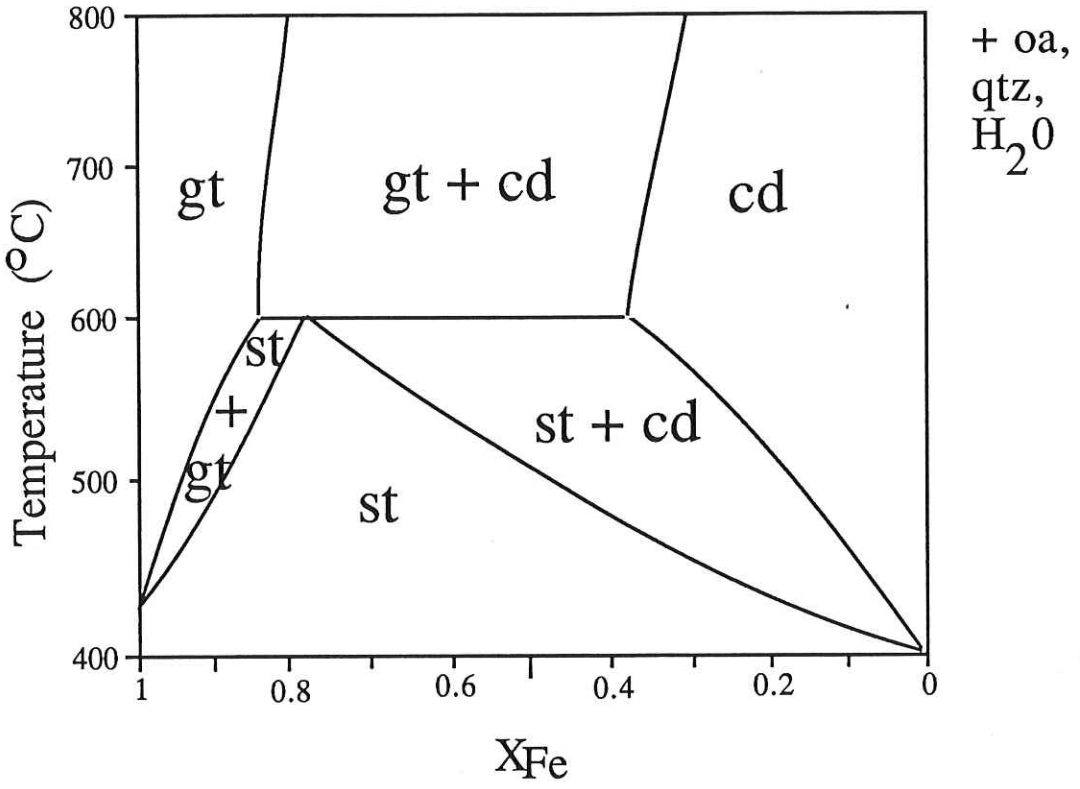

T-X diagram for the system FMASH at P = 4.5 kbar

sample	$X_{Fe,cd}$	$X_{Fe,st}$	$X_{Fe,gt}$
A911-48	35	80	-
A933-54	39	-	84

Figure 6: The T-X_{Fe} section in the FMASH system, and the compositions of coexisting minerals used to estimate the metamorphic field gradient.

2.4.3. Marble

A marble horizon of a few tens of metres in apparent thickness outcrops along the length of the area and is structurally repeated several times. Mineralogically it is dominated by calcite showing complex deformation textures. Additional minerals include scapolite, diopside, epidote, actinolite, garnet and vesuvianite. Vesuvianite is stabilised only under very water rich X_{fluid} conditions eg. $X_{CO2} < 0.1$ at 600°C and 4kbars (P.L.Dymoke, pers. comm.).

2.5 Summary of Critical Observations

The critical points which emerge from this metamorphic study of the Kanappa Hill area, and which place constraints on the processses responsible for the metamorphism are;

(1) peak temperatures reached at least 610°C, perhaps up to 630°C.

(2) a gradient of peak temperature vs distance of ~11-12°C/km is recorded near Kanappa Hill but this gradient drops to ~8-10°C/km 5km down grade.

(3) peak temperatures were reached coeval with a major crustal thickening event (D_2).

(4) P-T-t paths experienced by the rocks appear to have been closely isobaric during both prograde and retrograde metamorphism.

Such a set of observations is not unique but is common to many high T -low P terrains (DeYoreo, Lux and Guidotti, 1989; Sandiford and Powell, in press) and demands explanation.

3. INTERPRETATION OF THE METAMORPHIC PROCESSES

3.1 Theoretical Background

The conductive thermal response to thickening of the continental crust has been considered by various workers (England and Richardson, 1979; England and Thompson,

1984; England, 1978; Brewer, 1981) using a number of different deformation geometries. Numerical modelling has shown that homogeneous thickening of the lithosphere will result in significant crustal heating due to the extra internal heat production provided by the thicker crustal pile. But for geologically reasonable values of conductivity and heat source distribution the high temperatures at shallow to mid crustal levels often recorded in high T - low P terrains exceed predictions. Moreover the time scale for conductive relaxation is expected to be of the order of 100 Ma. and therefore peak metamorphic assemblages in a purely conductive regime will post date the compressive deformational event.

An alternative, inhomogeneous thickening geometry assumes that the base of the lithosphere is stripped off by mantle convection during the thickening event, an idea proposed by Houseman et al. (1981). This geometry allows for greater heat flux through the base of the crust yet numerical experiments by Sandiford (1989) and Sandiford and Powell (in press) using such a geometry suggest that at half crustal depth the maximum temperature attainable as a conductive response to the deformation is ~500°C.

Clearly, a purely conductive response to lithospheric thickening is not capable of satisfying conditions recorded in many highT-lowP terrains. Rather, a mechanism for rapidly advecting heat into the upper crust early in the history of the orogen is required. Two possibilities exist; (1) metamorphic fluid flow, and/or (2) emplacement of magmas. The presence of water-rich metamorphic fluids in the rocks of the Kanappa Hill area is indicated by the stability of vesuvianite. The following section evaluates the contribution of these fluids to the thermal budget of this terrain.

3.2. Fluid flow in the terrain

Prograde metamorphism of sedimentary rocks necessarily involves the release of significant volumes of fluid produced by dehydration reactions (Valley, 1986). As a potential carrier of both heat and matter the way in which this fluid escapes from the metamorphic pile is a central concern of metamorphic geology. Pervasive or channellised flow regimes will favour chemical homogeneity or heterogeneity respectively. In addition, pervasive fluid flow

may make a significant contribution to the thermal budget of a terrain. Indeed Wickham and Taylor (1985) propose pervasive flushing by convecting marine fluids as a major controlling factor of crustal melting in the low P Trois Seigneurs Massif, Pyrenees, France. This section is an attempt to estimate semi-quantitatively the contribution of fluid advection to the thermal perturbation recorded by the rocks in the Kanappa Hill area.

3.2.1. Theoretical Background

The fluids involved in metamorphism are derived from the progressive release of volatiles as sediments are subjected to increasing metamorphic grade. In pelitic rocks the volatiles released are dominantly H_2O and CO_2 with typical pelites losing 12 volume percent in H_2O and CO_2 at 500°C and 5 kbars (Walther and Orville, 1982) - a volume at least an order of magnitude higher than the typical porosity of schists, implying that the majority of volatiles are transported away from their site of release. These moving fluids then have the potential to advect both heat and matter.

Evaluation of the thermal consequences of fluid flow requires an estimate of the total fluid flux through a region and also the rate of flow which in turn requires the existence of some measurable physical trace sensitive to the fluid flow. Particularly useful tracers for H_2O and CO_2 rich fluids are the stable isotope values of carbon and oxygen. In particular, isotopic profiles across the boundaries between sedimentary units with initially very different isotopic signatures (e.g. schist and marble) provide an opportunity to evaluate fluid flow parameters. The utility of marble in a predominantly pelitic sequence is due to the fact that unaltered organic carbonate is enriched in heavy oxygen and heavy carbon with respect to clastic sediment. Thus we would expect a step function shaped stable isotope profile to be produced by a carbonate within a pelitic sequence. As diagenesis and metamorphism proceed, this initial profile will be subject to change, the nature of the changes being dependent on the processes acting. As a physical trace which is sensitive to these processes stable isotopic signatures can potentially provide information regarding mechanisms of mass transport in a metamorphic terrain.

Two contrasting mechanisms of mass transport are diffusion and advection. Diffusion will tend to smooth out any original isotopic anomaly while retaining its symmetry (Fig. 7a) Fluid advection on the other hand will tend to shift the anomaly in the direction of flow without altering its shape (Fig. 7c). In a terrain where neither mechanism is dominant a combined diffusive-advective profile is expected (Fig. 7b). A measure of the relative contribution of diffusion and advection is the Peclet Number (Bickle and MacKenzie,1987) defined, for concentration of a chemical species, as :

$$Pe = \frac{W_o \ h}{D_{eff}}$$

where W_o is the fluid flux, h is the thickness of boundary layer and D_{eff} is the effective diffusivity of the two phase material.

A Peclet Number greater than 10 implies advection is the dominant transport mechanism while a Peclet Number less than 1 implies diffusion is dominant. For Pe between 1 and 10 both mechanisms are significant and a combined diffusive-advective profile is the result.

3.2.2. Results

Twenty three samples were collected across a relatively fresh section of the Millendella Marble. The total width of the marble at this point is approximately 45 metres. The sampling interval was variable, being smaller at the margins of the band in order better to define the shape of the boundary layers. The carbon and oxygen stable isotope signatures of the samples were obtained by reacting the carbonate with acid and collecting the evolved CO_2 gas which was then analysed by mass spectroscopy. The results are shown in Figure 8.

The shape of these profiles is readily explicable by combined diffusion and advection i.e. a Peclet Number between 1 and 10. Both carbon and oxygen profiles show diffusive boundary layers on the margins of the marble with a broad, relatively flat plateau in the interior. Both profiles also show some asymmetry with the implied fluid flux being from east

Figure 7

Predicted isotopic profiles with pinned boundary conditions for various values of Pe. Dimensionless distance is plotted against dimensionless concentration for four progressive dimensionless times.

a) Pe=0. Symmetrical profiles due to diffusion only.

b) Pe=8. Slightly asymmetric profiles due to combined diffusion and advection.

c) Pe=20. Dominantly advective transport producing highly asymmetric profiles.

See Appendix D for the controlling equation.

a

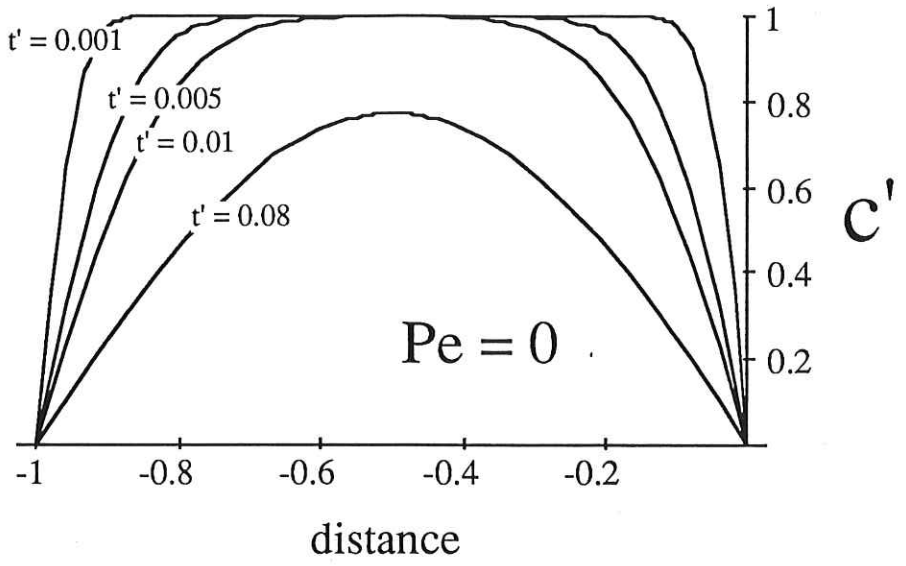
t' = 0.001
t' = 0.005
t' = 0.01
t' = 0.08
Pe = 0
1
0.8
0.6
0.4
0.2
c'
-1
-0.8
-0.6
-0.4
-0.2
distance

b

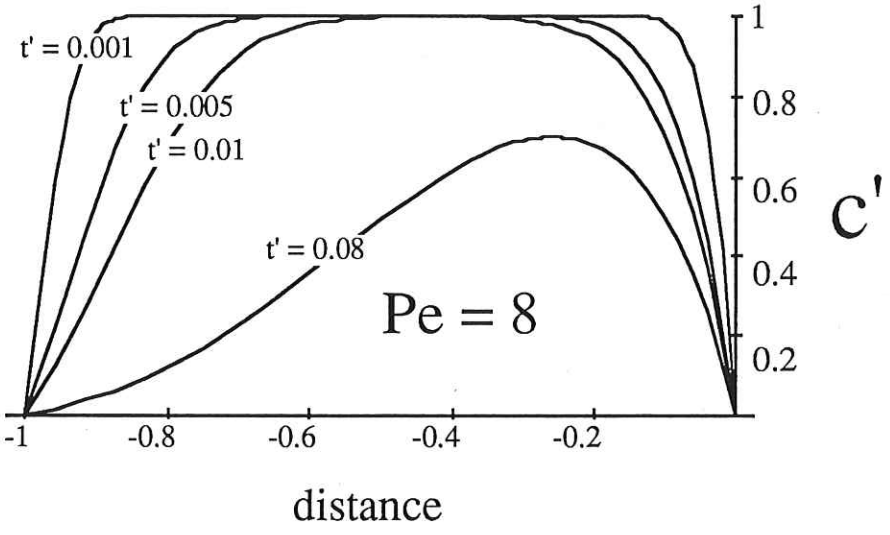
t' = 0.001
t' = 0.005
t' = 0.01
t' = 0.08
Pe = 8
1
0.8
0.6
0.4
0.2
c'
-1
-0.8
-0.6
-0.4
-0.2
distance

c

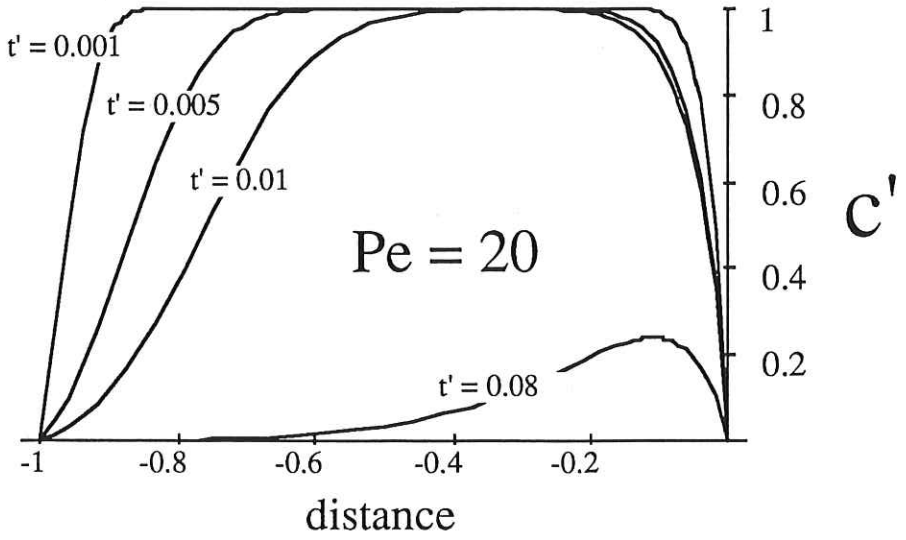
t' = 0.001
t' = 0.005
t' = 0.01
t' = 0.08
Pe = 20
1
0.8
0.6
0.4
0.2
c'
-1
-0.8
-0.6
-0.4
-0.2
distance

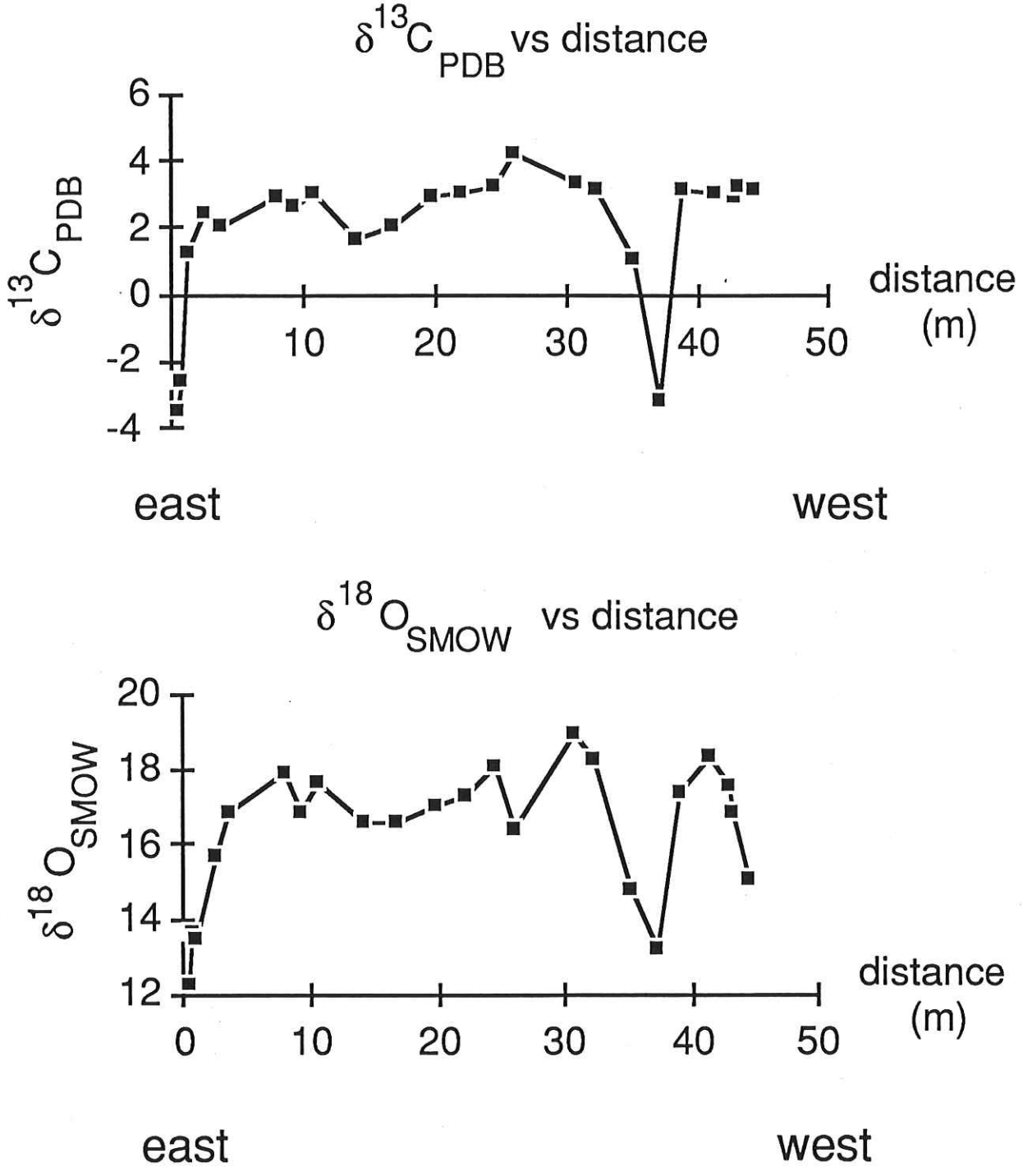

Figure 8

$\delta^{18}O$ and $\delta^{13}C$ vs distance profiles across a marble band 1 km South-East of Kanappa Hill. Both profiles show some assymetry with implied total fluid flux being East to West.

to west. This is simply a time-integrated fluid flux perpendicular to strike and says nothing regarding flux parallel to strike. Bickle and Baker (1990) consider fluid flow predominantly parallel to strike and channelled in the schists by modelling diffusion and advection of a step function with pinned boundary conditions. The results of such a flow regime are show in Figure 7 for various Peclet Numbers. The similarity of the observed profiles with the predicted profiles for Peclet Numbers between 1 and 10 is striking (Fig.7 and Fig.8).

The $\delta^{18}O$ profile shows broader boundary layers than the $\delta^{13}C$ profile. This suggests greater diffusive transport of oxygen than of carbon. The presence of vesuvianite in the sampled rocks suggests that the fluid compositions were very water- rich giving a higher effective diffusivity for oxygen than carbon thus lowering the Peclet Number for oxygen transport. The effect of the lower Peclet Number is to increase the relative contribution of diffusion over advection. Thus the fluid composition can explain the difference in boundary layer scales between the two profiles. The marked drop in δ values at distance ~38m coincides with a carbonate poor layer in the marble and is therefore considered to be a function of original isotopic composition.

A simple but important implication of the existence of this isotope profile is that fluid flow through the region has not been sufficient to homogenise the rocks isotopically. Bickle and MacKenzie (1987) show that advection of heat via metamorphic fluids requires very high fluid flux rates, of the order of $10^{-9}ms^{-1}$, and will necessarily cause alteration on length scales of several kilometres.

Comparison of measured profiles with predicted curves allows estimation of the Peclet number for the chemical transport in question. Peclet numbers for the measured profiles (Fig. 8) are estimated to lie between 1 and 10. Using this estimation allows calculation of the fluid flux across the profile via the relation,

$$W_o = \frac{\phi Pe\ D_f}{h}$$

where ϕ is the porosity, D_f is the diffusivity of the fluid, h is the length scale. Using the typical values for porosity and diffusivity (Bickle and MacKenzie, 1987; Bickle and Baker, 1990) of $\phi = .001$ and $D_f = 4.3 \times 10^{-8}$ and h = 50 m (the length scale of the profile), gives a value of $W_o \sim 9 \times 10^{-13}$ ms^{-1}, several orders of magnitude less than that required for crustal scale advection of heat in geologically reasonable time scales.

While fluid flow has had an important chemical and mineralogical part to play in the development of this terrain the flux rates were not sufficient to contribute significantly to the thermal budget. Consequently other means of rapidly advecting heat into the upper crust are required to explain the metamorphism.

3.3. Thermal Modelling

Having ruled out fluid flow as a major source of advected heat in the Kanappa Hill region, magmatic input of heat remains as the likely cause of the highT-lowP conditions. The occurrence of several large scale intrusive bodies (eg. Rathjen Gneiss, Palmer Granite, Reedy Creek Granodiorite) coincident with the highest grade of metamorphism is suggestive of such a causative relation. This section is a consideration of the metamorphic and deformational consequences of large scale magma input into the middle-upper crust.

Diffusion of heat from a cooling magmatic sill is described by the equation,

$$\frac{T}{T_o} = \frac{1}{2}\left(\text{erf}\left(\frac{\xi+1}{2\tau^{0.5}}\right) - \text{erf}\left(\frac{\xi-1}{2\tau_0^{0.5}}\right)\right)$$

where ξ is x/a, x is the vertical distance from the centre of the sill, a is half thickness of sill, τ is dimensionless time ($\kappa t / a^2$ where t is time), κ is thermal diffusivity, and T_o is the difference between the temperature of the magma and the country rock ($T_0 = T_{magma} - T$ country rock). (Wickham and Oxburgh, 1987)

It is informative to consider the relation between peak temperature in the country rock and distance from the sill predicted by this equation. If temperature is plotted against distance

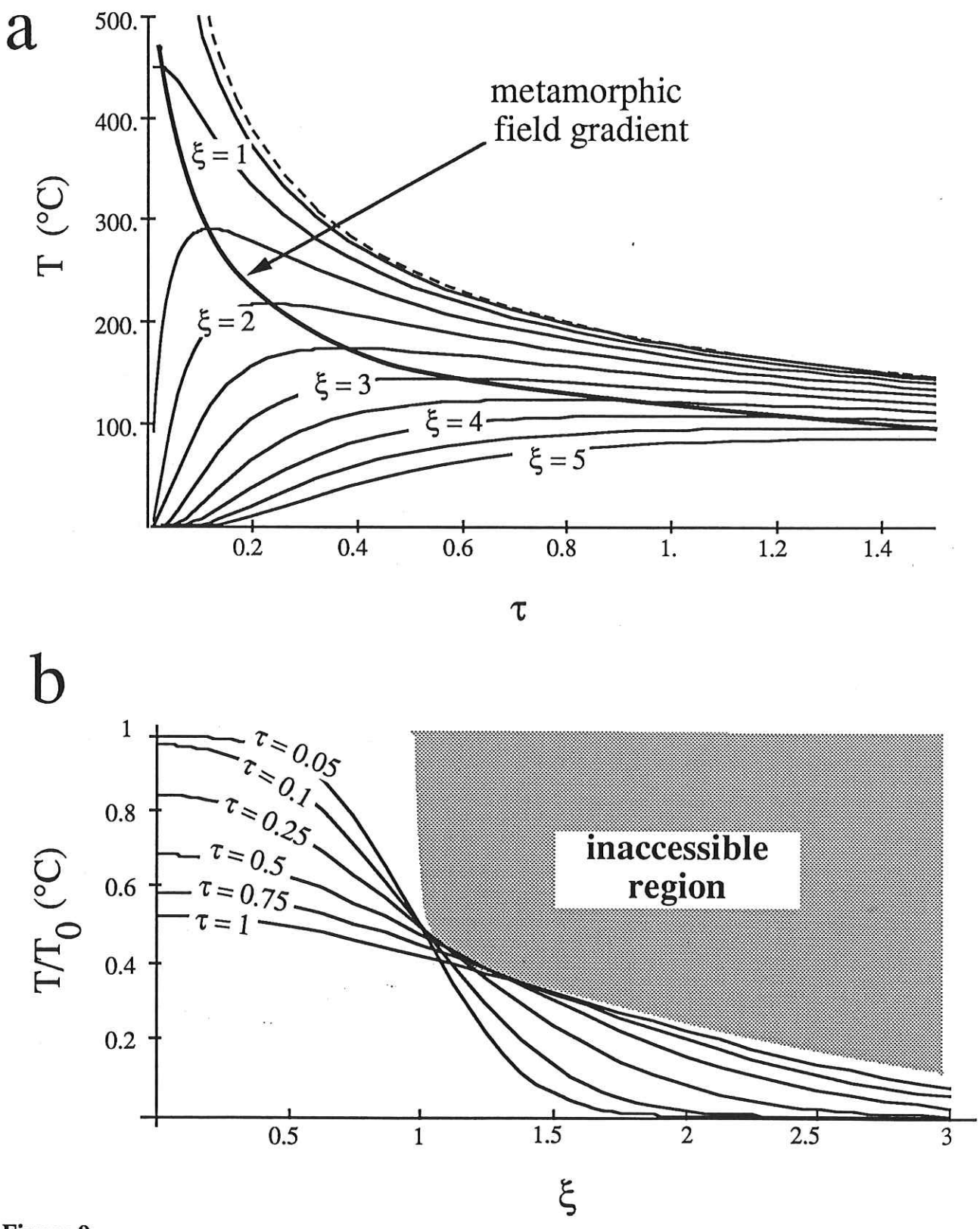

Figure 9
a) Temperature plotted against dimensionless time for increasing distances from a magmatic sill. The bold line is the locus of peak temperatures with distance (the metamorphic field gradient) and shows an exponential decrease with distance from the sill.

b) Dimensionless temperature plotted against dimensionless distance at distinct times. The enveloping curve, defining the boundary of the shaded, inaccesible region also defines the metamorphic field gradient.

for a series of discrete times, the set of peak temperatures forms an enveloping curve which defines the predicted metamorphic field gradient. The form of this curve is an exponentially decreasing function with distance from the sill. The conclusion from petrologic evidence in section 2.4 (metamorphism) that the field gradient increases up grade is therefore consistent with the metamorphism being due to diffusive heat from a local intrusive.

The source of the magma, however, and the relation between emplacement and deformation remain to be resolved. The numerical experiments of Sandiford and Powell (in press) show that even where the base of the lithosphere is stripped away during deformation a purely conductive thermal response will not raise mid crustal temperatures sufficiently to explain many high T-low P terrains, including the Eastern Mount Lofty Ranges. However, at the base of the crust, potential temperatures may exceed 1000°C creating the possibility of large scale lower crustal melting. This in turn allows for rapid advection of heat into middle and upper crustal levels as the melts segregate and rise. In this scenario upper crustal temperatures will locally be raised well above the 500°C limit predicted due to conductive equilibration. What remains critically in question, however, is whether this process of melt generation, segregation and emplacement can occur over time intervals short enough to allow for peak metamorphic temperatures at 10-15km depth to be reached during the compressive event.

In order to answer this question quantitatively a numerical thermo-mechanical model of the lithosphere has been developed. The rheological and mechanical aspects of the model are detailed elsewhere (Martin, 1990) but are outlined briefly below. More attention is paid here to the thermal aspects and the implications for metamorphism.

3.3.1. The Numerical Model

The aim of the model is to provide an insight into the thermal and mechanical response of the lithosphere to upper crustal magma emplacement. Melt emplacement at crustal levels appropriate to low P terrains has the potential for dramatic mechanical effects since crustal strength is concentrated at such depths.

In the model the rheology of the lithosphere is greatly simplified by considering the crust to be quartz dominated and the mantle lithosphere to be olivine dominated. Experimental work (Shelton and Tullis, 1981) has shown such an approximation to be valid provided the mineral in question makes up at least 30% of the rock.

In the upper crust, where confining pressures are low, crustal strength is linearly dependent on confining pressure and is given by Byrelee's law;

$$\sigma_1 - \sigma_3 = c + \mu \rho g z \tag{3.1}$$

where c is a material constant, μ is the coefficient of friction, ρ is the density, z is the depth. At greater depths, below the brittle/ductile transition, deformation will be ductile and crustal strength dependent on both temperature and strain rate according to the power creep law;

$$\sigma_1 - \sigma_3 = \left(\frac{\dot{\varepsilon}}{A}\right)^{1/n} \exp\left(\frac{Q}{n\ R\ T}\right) \tag{3.2}$$

where $\dot{\varepsilon}$ is the strain rate, A is a material constant, Q is the activation energy, R is the gas constant, T is the temperature.

Fundamental to any understanding of the mechanics of orogenesis, and interpretation of the predictions of the model, is the concept of balance between driving and buoyancy forces. An orogen will be stable ie. not actively deforming, only when the following relation is satisfied:

$$F_{dc} = F_b + F_{str} \tag{3.3}$$

where F_{dc} is the compressional driving force, F_b is the buoyancy force and F_{str} is the lithospheric strength.

An alternative expression of this relation is;

$$F_{edc} = F_{dc} - F_b = F_{str} \tag{3.4}$$

where F_{edc} is referred to as the effective driving force (e.g., Sandiford and Powell, 1990). Compressive deformation can proceed only when the effective driving force exceeds lithospheric strength. Driving forces are external forces arising from such gross tectonic processes as ridge push and slab pull.

Total lithospheric strength is calculated by integrating strength, as given by the power law creep and Byrelee's laws, with respect to depth. Consequently, lithospheric strength is dependent on both the thermal regime present and the strain rate. Lithospheric strength is increased at high strain rates but decreased at high temperatures.

Buoyancy forces, induced by differences in density structure with depth between deformed and undeformed lithosphere, act so as to reduce any topography on both the surface and base of the crust and hence oppose driving forces. As topographic relief increases so too will the buoyancy forces.

The numerical model assumes driving force is constant throughout and acts initially on an undeformed lithosphere with no topography. Hence initially buoyancy force is zero and if the imposed driving force exceeds lithospheric strength then compressive deformation will occur. As deformation proceeds crustal thickening will produce topography and buoyancy force will progressively increase. In addition the lithospheric strength will be modified by the evolving thermal regime. Since strain rate also modifies lithospheric strength the deformation will proceed only at strain rates low enough for effective driving force to exceed F_b. Theoretically, continued strain will eventually result in buoyancy forces being equal and opposite to driving force causing deformation to cease. At this stage the lithosphere has reached its potential energy maximum and has no internal strength, topography being maintained simply by the continued action of the external driving force. For any constant value of driving force an orogen therefore has a limit to crustal thickening (f_c) imposed by its density depth profile. Once this limiting f_c value is reached vertical strain must cease and further shortening is accommodated by outward building of the terrain. The Tibetan Plateau may be an example of this process (England and Houseman, 1988). For heterogeneous

lithospheric strain geometries involving efficient convective stripping of the lower lithosphere f_c is limited to relatively small thickening strains. For F_{dc} values of 5×10^{12} a limit on f_c of ~1.6 is suggested by Sandiford and Powell (1990).

The distribution of heat in the lithosphere, via its control on strength and therefore force balance, plays a critical role in the strain history of an orogen. In the absence of rapid heat transfer (eg. fluid or melt migration) heat distribution will be subject only to slow, conductive change and consequently lithospheric strength and strain rate also change steadily. Under the condition of constant applied driving force only rapid changes in thermal structure, as may be effected by melt migration, have the potential to cause a large imbalance between effective driving force and strength. A large imbalance of force will result in a rapid increase in strain rate until buoyancy forces are sufficient to redress the balance. Importantly, as the magnitude of buoyancy forces approaches that of the driving force, lithospheric strength approaches zero. If melts are intruded into the crust at this stage, when the strength term is relatively insignificant, their effect on force balance, and consequently strain rate, will be much reduced.

Output from the model as strain vs time plots illustrates this point (Fig. 10a, b). If melts are generated in the lower crust simply in response to conductive heating the strain history of the orogen is very different to that resulting from advective heat input from the asthenosphere. In the first case, where melting is a response to deformation, the time taken for conductive heating to generate lower crustal melts allows the orogen to approach its potential strain maximum before melt emplacement at shallow crustal levels. Consequently melt emplacement has very little deformational effect relative to the total strain history . Figure 10a suggests ~5% crustal thickening is a direct result of melt emplacement while ~50% thickening has already occurred at the time of emplacement. Since peak metamorphic temperatures at shallow crustal levels will follow intrusion, peak mineral growth cannot be associated with the major crustal thickening event.

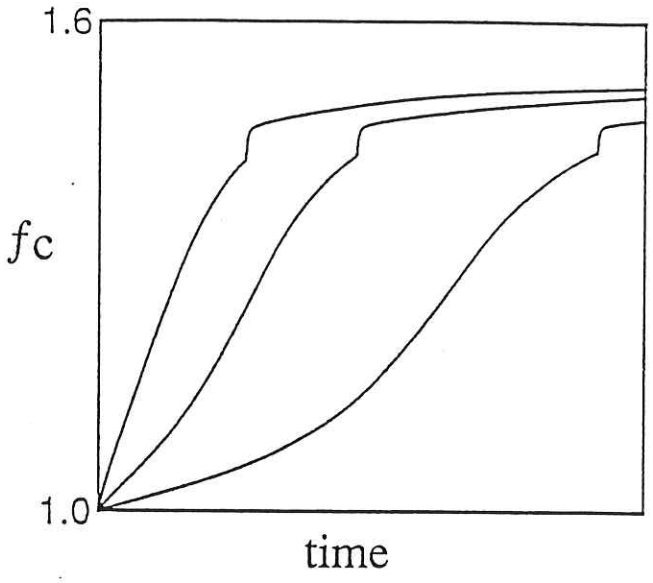

a

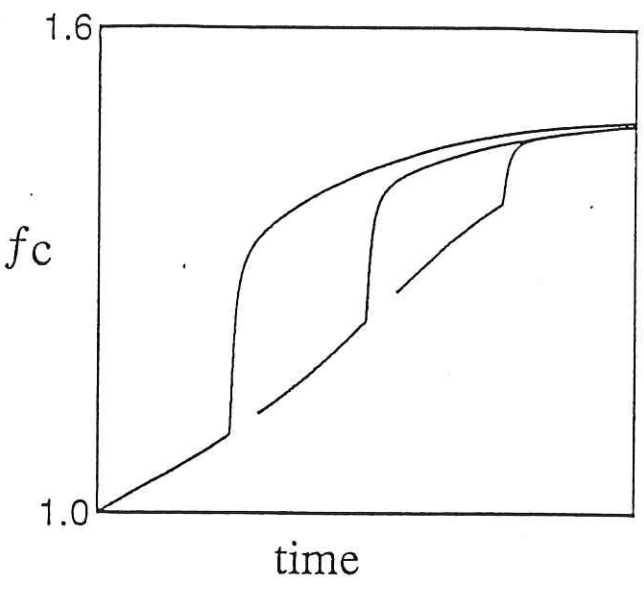

b

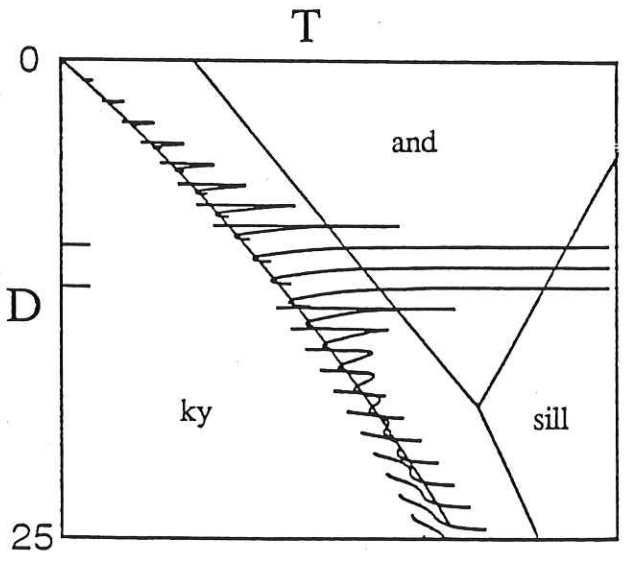

c

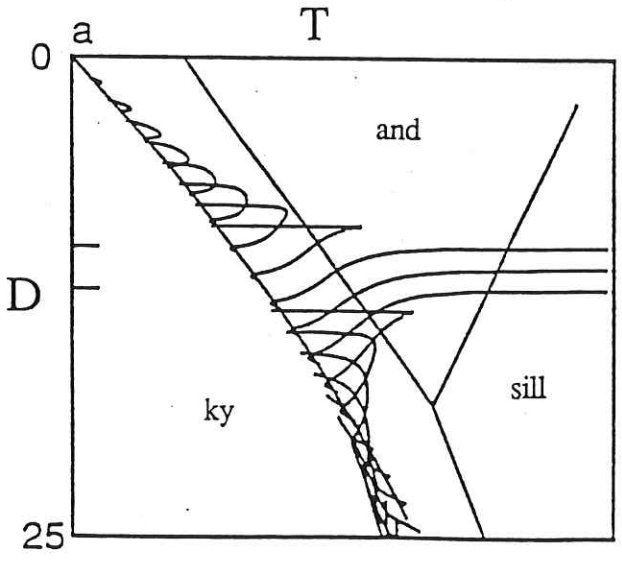

d

The observation of peak temperature mineral growth within a pervasive compressional deformation fabric in the Kanappa Hill area is therefore clear evidence against conductive equilibration of thickened crust being the cause of the metamorphism.

Asthenospheric heat input is an alternative heat source to conductive equilibration and potentially can give rise to a very different strain history. Asthenospheric magma rising through the cooler and denser lithospheric mantle is likely to pool at the density contrast at the base of the crust. In response deep crustal melts may be generated and rise to mid-upper crustal levels. In this case the timing of advective heat input is not constrained to late in the compressive tectonic cycle. If emplacement occurs early in a compressive regime, the dramatic thermal weakening of the lithosphere has the potential to effect sudden and rapid vertical strain (Fig. 10 b). Major crustal thickening is therefore an effect, rather than a cause, of melt emplacement. In mid-upper levels of the crust deformation and peak metamorphism are predicted to occur together during the thermal pulse produced by the intrusion, a prediction which accords with observation from the Kanappa Hill area.

P-T-t paths for crust subject to magma emplacement under a compressive tectonic region are plotted in Figures 10 c,d. In contrast to the smooth anti-clockwise paths predicted in the absence of advective heat transfer (England and Thompson, 1984) these show an almost isobaric "spike" followed initially by isobaric cooling then by increasing pressure.

The reconstructed portion of the P-T-t path for the Kanappa Hill rocks (Figs.4 & 5 FMASH section prograde, KFMASH retrograde section) are consistent with the quantitative form of these predicted paths. The portions of the paths reconstructed from petrologic considerations are close to peak temperature and illustrate near-isobaric heating and cooling consistent with them being due to a sharp local pulse - the "spike" in the predicted P-T-t curves.

The aluminosilicate stability fields have been overlain on the P-T-t paths to give an indication of the predicted metamorphic grades. For a single sill of 2 km thickness at 850°C

mid-upper crustal metamorphic peaks are predicted to lie in the andalusite stability field, with sillimanite grade reached only in close proximity to the sill itself (approximately 2 km). This is somewhat at odds with field observation of a rather more extensive sillimanite grade region east of Springton, S.A.. However, since our knowledge of the present sub-surface or eroded extent of local granitic intrusives e.g. Rathjen Gneiss, Cooke Hill Granite is poor, it is structurally possible that boundaries of the observed sillimanite grade zone are of the order of only 2 km from the intrusives.

Since the Palmer Granite appears to post-date the Rathjen Gneiss (Martin, 1990), it is likely that more than one episode of granitic emplacement occurred. The combined effect of several intrusive episodes within a few Ma. could potentially raise the country rock to sillimanite grade over a wider area than that shown in Figures 10 c,d.

In conclusion, model predictions of the thermo-mechanical response of the crust to advective, asthenospheric heat input are in close agreement with field observation.

4. DISCUSSION AND CONCLUSIONS

Asthenospheric melt generation is generally regarded as a response to decompression rather than compression. Thus although the metamorphic record is consistent with a thermal model which invokes asthenosphere melt input, the generation of such melts in a compressive regime is somewhat enigmatic.

Foden et.al. (1990) recognise three phases of Cambro-Ordovician magmatic activity, being syn-sedimentary, syn-deformational, and post-tectonic. The pre-deformational magma is dominantly mafic with a sub-crustal origin. Mafic underplating of the crust is proposed to have occurred through the Adelaidean. Melting of this mafic underplate is proposed during the pre-Delamerian extensional event with these mafic melts rising into the upper crust during the Delamerian Orogeny.

This scenario fits comfortably with the conclusion that the high T-low P metamorphism in the Eastern Mount Lofty Ranges resulted from rapid sub-crustal heat input early in the compressive Delamarian Orogeny.

From all the foregoing evidence the following points seem inescapable;

(1) High T-low P metamorphism in the Kanappa Hill Area occurred as a consequence of rapid heat transfer into the upper crust and was not simply due to conductive thermal relaxation after crustal thickening.

(2) Estimation of fluid flux rules out pervasive flushing by hot metamorphic fluids as the responsible heat transfer mechanism.

(3) Synorogenic intrusives emplaced in the upper crust were the source of the high metamorphic temperatures recorded in the Kanappa Hill Area.

(4) Advective heat input from subcrustal levels is invoked on theoretical grounds as the likely source of these intrusives.

ACKNOWLEDGEMENTS

I must wholeheartedly thank my supervisor, Mike Sandiford, firstly for rekindling my interest in geology last year and offering me this project, and secondly for the interest, enthusiasm and guidance he has provided this year. I also thank his co-workers, Peter Dymoke and Kurt Stuwe, for their friendship, encouragement and advice and Peter in particular for explanation of his petrogenetic grids. The PhD students, Simon, Kathy, Graeme, Jo, Bunge and Martin also contributed in various ways towards making the year both enjoyable and academically rewarding.

My fellow honours students have provided plenty of moral support and great friendship-I thank them all and hope I was able to do the same in return.

Mr Starkey (Green Gables) and Mr Newman (Clovelly) are thanked for allowing me access to their properties during the field work.

Technical help for this project has been provided by Keith Turnbull (stable isotope analyses), Wayne Mussared and Geoff Trevelyan (thin section preparation), Hugh Rosser (microprobe analyses) and Sherry Proferes (drafting). My Father spent considerable time proof reading the text and making constructive criticisms of the argument.

Lastly, but perhaps most importantly, I thank my parents who have given me unqualified support over four years of university study. Without that understanding, security and encouragement it is doubtful whether I would ever have completed those years.

REFERENCES

Abbas SAF (1972) Granitic and migmatitic rocks of the Cooke Hill area, South Australia, and their structural setting. MSc thesis, University of Adelaide (unpublished)

Allen RV (1977) Metamorphic phase relations in the Kanmantoo. Honours thesis, University of Adelaide (unpublished)

Arnold J (1989) Petrogenesis of cordierite-orthoamphibole assemblages from the Springton region, Mount Lofty Ranges. Honours thesis, University of Adelaide (unpublished)

Arnold J, Sandiford M (1990) Petrogenesis of cordierite-orthoamphibole assemblages from the Springton region, South Australia. *Contrib Mineral Petrol* (in press)

Bickle MJ, Baker J (1990) Advective-diffusive transport of isotopic fronts: an example from Naxos, Greece. *Earth Planet Sci Lett* 97: 78-93

Bickle MJ, MacKenzie D (1987) The transport of heat and matter by fluids during metamorphism. *Contrib Mineral Petrol* 95: 384-392

Boyer SE, Elliot D (1982) Thrust systems. *American Assoc Petrol Geol Bull* 66: 1196-1230

Brewer J (1981) Thermal effect of thrust faulting. *Earth Plant Sci Lett* 56: 233-244

Butler RWH (1982). Hanging wall strain; a function of duplex shape and footwall topography. *Tectonophysics* 83 ; 235-247

Cooper BJ (1989). The Early Cambrian Milendella Limestone Member (Kanmantoo Group), a stratigraphic marker horizon in the Karinya Syncline. *South Australia. Geological Survey. Quaterly Geological Notes,* 109: 15-23

DeYoreo, JJ, Lux DR, Guidotto CV (1989) The role of crystal anatexis in magma migration in the thermal evolution of regions of thickened continental crust. In; Daly JS, Cliff RA,

Yardley BWD (eds) Evolution of metamorphic belts, *Geol Socy Spec Lond Publ 43*,, 187-202

Dymoke P, Sandiford M (Submitted) Phase relations of Buchan facies series pelitic assemblages: calculations and applications to the Mount Lofty Ranges, South Australia. Submitted to *Contrib Mineral Petrol*

England PC (1987) Some thermal considerations of the Alpine metamorphism, past present and future. *Tectonophysics* 46: 21-40

England PC, Houseman, G, (1988) The mechanics of the Tibetan Plataeu, *Phil Trans Roy Soc Lond,* A326: 301-320.

England PC, Richardson SW (1977) The influence of erosion upon the mineral facies of rocks from different metamorphic environments. *J Geol Soc, London* 134 :201-213

England PC, Thompson AB(1984) Pressure-temperature-time paths of regional metamorphism I. Heat transfer during the evolution of thickened continental crust. *J Petrol* 25: 894-928

Ferry JM, Spear FS (1978) Experimental calibration of the partitioning of Fe and Mg between biotite and garnet. *Contrib Mineral Petrol:* 13-117

Fleming PD (1971) Metamorphism and folding in the Mt Lofty Ranges, South Australia, with particular reference to the Dawesley-Kanmantoo area. PhD thesis University of Adelaide (unpublished)

Houseman G, McKenzie D, Molnar P (1981) Convective instability of a thickened boundary layer and its relevance for the thermal evolution of continental convergence belts. *J. Geophys. Res.* 86: 6115-6132

Jenkins RJF (1990) The Adelaide Fold Belt: tectonic reappraisal. In: Proterozoic and Early Palaeozoic geology of the Adelaide Geosyncline, Geological Society of Australia, Special Publication 16 (Daily Volume), 396-420

Mancktelow NS (1979) The structure and metamorphism of the Southern Adelaide Fold Belt. PhD thesis, University of Adelaide (unpublished)

Martin N (1990) A coupled thermo-mechanical model for deformation in high temperature-low pressure metamorphic terrains: implications for the Palmer Region, Southern Adelaide Fold Belt.,Honours Thesis, University of Adelaide (unpublished)

Mills KJ (1964) Structural petrology East of Springton, SA. PhD thesis, University of Adelaide (unpublished)

Offler R, Fleming PD (1968) A synthesis of folding and metamorphism in the Mount Lofty Ranges, South Australia. *J Geol Soc Aust* 15:245-266

Powell R, Holland TJB (1988) An internally consistent dataset with uncertainties and correlations: 3. Applications to geobarometry, worked examples and a computer program. *J Met Geol* 6: 173-204

Sandiford M (1989) Secular trends in the thermal evolution of metamorphic terrains. *Earth Planet Sci Lett* 95: 85-96

Sandiford M, Oliver RL, Mills KJ, Allen RV (1990) A cordierite-staurolite-muscovite association, East of Springton, Mount Lofty Ranges; Implications for the metamorphic evolution of the Kanmantoo Group. In: Proterozoic and Early Palaeozoic geology of the Adelaide Geosyncline, Geological Society of Australia, Special Publication 16 (Daily Volume) pp 483-495

Sandiford M, Powell R, (1990) Some isostatic and thermal consequences of the vertical strain geometry in convergent orogens. *Earth Planet Sci lett,* 98, 154-165.

Sandiford M, Powell R (in press) Some remarks on high temperature-low pressure metamorphism in convergent orogens. *J Met Geol* (in press)

Shelton ,G, Tullis, J, (1981) Experimental flow laws for crustal rocks, *EOS* 62 396.

Valley JW (1986) Stable isotope geochemistry of metamorphic rocks. In: Valley JW, Taylor HP, O'Neil JR (eds) Stable isotopes in high temperature geological processes; Reviews in Mineralogy, *Mineral Soc Amer,* vol 16, pp 445-489.

Walther JV, Orville PM (1982) Volatile production and transport in regional metamorphism. *Contrib Mineral Petrol* 79: 252-257

Wickham SM, Oxburgh ER (1987) Low-pressure regional metamorphism in the Pyrenees and its implications for the thermal evolution of rifted continental crust. *Phil.Trans. Roy. Soc. Lond.* A321: 219-242

Wickham SM, Taylor HP (1985) Stable isotopic evidence for large-scale seawater infiltration in a regional metamorphic terrain; the Trois Seigneurs Massif, Pyrenees, France. *Contrib Mineral Petrol* 91: 122-137

APPENDIX A

Stable Isotope Data from Vesuvianite Creek, Kanappa Hill

SAMPLE	distance	δ13PDB	δ18PDB	δ18VSMOW
933-56	0.35	-3.5	-18.15	12.2
933-57	0.62	-2.64	-16.72	13.67
933-58	1.06	1.29	-16.95	13.44
933-59	2.45	2.42	-14.77	15.7
933-60	3.59	2.07	-13.65	16.84
933-61	7.96	2.92	-12.64	17.88
933-62	9.33	2.63	-13.67	16.82
933-63	10.67	3	-12.86	17.65
933-64	14.12	1.65	-13.94	16.54
933-65	16.77	2.06	-13.97	16.51
933-66	19.87	2.93	-13.48	17.01
933-67	22.08	2.98	-13.26	17.24
933-68	24.59	3.22	-12.49	18.03
933-69	26.14	4.16	-14.09	16.38
933-70	30.71	3.3	-11.63	18.92
933-71	32.43	3.08	-12.33	18.2
933-72	35.18	1.07	-15.64	14.79
933-73	37.13	-3.23	-17.21	13.17
933-74	38.93	3.1	-13.12	17.38
933-75	41.34	2.98	-12.24	18.29
933-76	42.86	2.88	-13	17.51
933-77	43.2	3.21	-13.67	16.82
933-78	44.37	3.08	-15.37	15.06

Marble band is 45m wide. Distances are from the Eastern margin

APPENDIX B Microprobe data

Biotite (Recalculated to 11 Oxygens)

	933-52		933-53	933-54		890-134		930-30		933-45
SiO2	33.05	33.83	34.58	34.15	34.40	31.60	33.60	33.61	34.49	32.08
TiO2	1.60	2.02	1.33	1.86	2.30	2.60	2.99	1.82	1.97	1.10
Al2O3	18.23	18.40	16.24	16.94	17.02	17.44	17.50	16.19	16.73	18.42
FeO	22.89	23.53	18.50	20.67	19.90	21.15	20.78	18.94	19.20	19.62
MnO	0.00	0.00	0.00	0.00	0.00	0.00	0.00	0.00	0.00	0.00
MgO	6.49	6.50	11.30	9.39	9.64	8.72	7.92	9.67	10.08	14.40
CaO	0.00	0.00	0.15	0.00	0.00	0.00	0.00	0.00	0.00	0.10
Na2O	0.50	0.55	0.39	0.24	0.34	0.28	0.25	0.28	0.42	0.29
K2O	8.96	9.02	7.66	8.97	8.88	7.74	9.54	8.00	8.79	5.15
Total	91.7	93.9	90.2	92.2	92.5	89.5	92.6	88.5	91.7	91.2
Si	2.678	2.679	2.764	2.716	2.715	2.597	2.675	2.755	2.737	2.522
Ti	0.097	0.120	0.080	0.111	0.137	0.161	0.179	0.112	0.118	0.065
Al	1.741	1.718	1.530	1.589	1.584	1.690	1.643	1.564	1.565	1.707
Fe2+	1.551	1.559	1.237	1.375	1.314	1.454	1.384	1.298	1.274	1.290
Mn	0.000	0.000	0.000	0.000	0.000	0.000	0.000	0.000	0.000	0.000
Mg	0.784	0.767	1.346	1.113	1.134	1.068	0.940	1.181	1.192	1.687
Ca	0.000	0.000	0.013	0.000	0.000	0.000	0.000	0.000	0.000	0.008
Na	0.079	0.084	0.060	0.037	0.052	0.045	0.039	0.044	0.065	0.044
K	0.926	0.911	0.781	0.910	0.894	0.812	0.969	0.837	0.890	0.516
Total	7.856	7.839	7.812	7.852	7.829	7.825	7.828	7.792	7.840	7.840

Biotite (Recalculated to 11 Oxygens)

	933-45	890-138		
SiO2	37.77	35.23	35.01	36.73
TiO2	1.28	1.23	2.03	0.16
Al2O3	16.07	17.07	16.57	16.33
FeO	16.00	17.15	17.44	22.12
MnO	0.00	0.00	0.00	0.00
MgO	11.89	11.85	10.45	8.57
CaO	0.31	0.09	0.00	0.00
Na2O	0.36	0.73	0.48	0.17
K2O	7.79	7.06	7.52	7.11
Total	91.5	90.4	89.5	91.2
Si	2.913	2.772	2.795	2.916
Ti	0.074	0.073	0.122	0.010
Al	1.461	1.583	1.559	1.528
Fe2+	1.032	1.128	1.164	1.469
Mn	0.000	0.000	0.000	0.000
Mg	1.367	1.390	1.243	1.014
Ca	0.026	0.008	0.000	0.000
Na	0.054	0.111	0.074	0.026
K	0.766	0.709	0.766	0.720
Total	7.693	7.774	7.724	7.683

Staurolite (Recalculated to 48 Oxygens)

	933-52		933-30	
SiO2	26.92	27.10	25.94	25.97
TiO2	0.00	0.00	0.64	0.66
Al2O3	52.84	53.35	52.89	52.75
FeO	12.67	12.72	13.80	13.29
MnO	0.00	0.00	0.00	0.00
MgO	1.08	1.24	1.91	1.70
CaO	0.00	0.00	0.00	0.00
Na2O	0.44	0.50	0.43	0.36
K2O	0.00	0.00	0.00	0.00
Total	94.0	94.9	95.6	94.7
Si	8.080	8.054	7.725	7.781
Ti	0.000	0.000	0.143	0.149
Al	18.698	18.692	18.569	18.632
Fe2+	3.181	3.161	3.437	3.330
Mn	0.000	0.000	0.000	0.000
Mg	0.483	0.549	0.848	0.759
Ca	0.000	0.000	0.000	0.000
Na	0.256	0.288	0.248	0.209
K	0.000	0.000	0.000	0.000
Total	30.699	30.744	30.971	30.859

Gedrite (Recalculated to 23 Oxygens)

	933-53		890-135							
SiO2	39.46	39.12	44.77	44.09	44.48	47.66	48.34	43.61	44.69	46.64
TiO2	0.15	0.11	0.35	0.24	0.31	0.28	0.30	0.30	0.32	0.22
Al2O3	16.09	16.80	10.94	12.18	11.75	7.79	7.13	12.26	11.24	9.06
FeO	26.62	27.27	26.11	27.71	25.93	26.12	26.70	26.14	26.05	26.39
MnO	0.00	0.00	0.00	0.00	0.00	0.00	0.00	0.00	0.00	0.00
MgO	9.40	9.43	11.61	11.17	11.71	12.88	13.29	11.03	11.57	12.27
CaO	0.00	0.00	0.00	0.08	0.00	0.00	0.00	0.00	0.00	0.00
Na2O	1.98	2.01	1.50	1.57	1.61	1.10	0.94	1.63	1.35	1.18
K2O	0.00	0.00	0.00	0.06	0.00	0.00	0.00	0.05	0.00	0.00
Total	93.7	94.7	95.3	97.1	95.8	95.8	96.7	95.0	95.2	95.8
Si	6.225	6.124	6.864	6.691	6.779	7.230	7.277	6.720	6.849	7.098
Ti	0.018	0.013	0.040	0.027	0.036	0.032	0.034	0.035	0.037	0.025
Al	2.993	3.101	1.978	2.179	2.111	1.393	1.265	2.227	2.031	1.625
Fe2+	3.512	3.570	3.348	3.517	3.305	3.314	3.361	3.369	3.339	3.359
Mn	0.000	0.000	0.000	0.000	0.000	0.000	0.000	0.000	0.000	0.000
Mg	2.210	2.200	2.653	2.526	2.660	2.912	2.982	2.533	2.643	2.783
Ca	0.000	0.000	0.000	0.013	0.000	0.000	0.000	0.000	0.000	0.000
Na	0.606	0.610	0.446	0.462	0.476	0.324	0.274	0.487	0.401	0.348
K	0.000	0.000	0.000	0.012	0.000	0.000	0.000	0.010	0.000	0.000
Total	15.564	15.618	15.329	15.428	15.367	15.204	15.194	15.380	15.299	15.238

Gedrite (Recalculated to 23 Oxygens)

	890-135		890-138				933-45		933-30	
SiO2	48.54	48.12	40.27	40.22	40.50	40.96	41.26	41.26	40.94	37.38
TiO2	0.16	0.20	0.36	0.19	0.23	0.16	0.31	0.23	0.00	0.25
Al2O3	6.64	7.71	16.42	16.63	16.03	16.06	16.61	16.41	16.54	22.70
FeO	26.49	26.29	25.72	26.12	26.04	25.55	27.38	27.84	20.72	18.08
MnO	0.00	0.00	0.00	0.20	0.11	0.12	0.00	0.00	0.00	0.00
MgO	12.97	12.96	9.88	9.75	9.87	10.29	10.77	10.46	6.82	6.17
CaO	0.00	0.00	0.00	0.00	0.00	0.00	0.00	0.00	0.43	0.28
Na2O	0.90	1.10	1.80	1.92	1.61	1.80	1.86	1.74	0.26	0.42
K2O	0.00	0.00	0.00	0.00	0.00	0.00	0.00	0.00	1.32	4.13
Total	95.7	96.4	94.5	95.0	94.4	94.9	98.2	97.9	87.0	89.4
Si	7.373	7.255	6.254	6.228	6.301	6.318	6.198	6.225	6.717	6.015
Ti	0.018	0.023	0.042	0.022	0.027	0.019	0.035	0.026	0.000	0.030
Al	1.189	1.370	3.006	3.036	2.940	2.920	2.942	2.919	3.199	4.306
Fe2+	3.365	3.315	3.341	3.382	3.388	3.296	3.440	3.513	2.843	2.433
Mn	0.000	0.000	0.000	0.026	0.014	0.016	0.000	0.000	0.000	0.000
Mg	2.936	2.912	2.287	2.250	2.288	2.365	2.411	2.352	1.668	1.480
Ca	0.000	0.000	0.000	0.000	0.000	0.000	0.000	0.000	0.076	0.048
Na	0.265	0.322	0.542	0.576	0.486	0.538	0.542	0.509	0.083	0.131
K	0.000	0.000	0.000	0.000	0.000	0.000	0.000	0.000	0.276	0.848
Total	15.147	15.197	15.472	15.521	15.445	15.472	15.567	15.544	14.862	15.291

Garnet (Recalculated to 12 Oxygens)										
	933-52	933-53		933-54		933-23		933-30		
SiO2	35.59	36.36	36.16	35.51	36.48	37.12	38.12	34.50	34.88	36.22
TiO2	0.00	0.00	0.00	0.00	0.00	0.44	0.48	0.00	0.00	0.00
Al2O3	19.75	19.91	19.99	19.47	19.75	17.88	18.17	19.12	18.97	19.94
FeO	39.30	37.76	36.66	37.24	37.44	6.22	6.15	35.42	35.23	37.17
MnO	0.54	0.00	0.00	0.26	0.21	0.75	0.77	0.64	0.70	0.64
MgO	2.43	3.49	4.43	3.78	4.03	0.00	0.00	4.20	4.31	4.03
CaO	0.22	0.38	0.43	0.35	0.52	34.00	34.74	0.27	0.37	0.09
Na2O	0.32	0.21	0.35	0.29	0.53	0.15	0.20	0.23	0.41	0.25
K2O	0.00	0.00	0.07	0.00	0.07	0.00	0.00	0.00	0.00	0.00
Total	98.2	98.1	98.1	96.9	99.0	96.6	98.6	94.4	94.9	98.3
Si	2.974	3.002	2.977	2.978	2.988	2.991	3.003	2.962	2.977	2.984
Ti	0.000	0.000	0.000	0.000	0.000	0.027	0.028	0.000	0.000	0.000
Al	1.946	1.938	1.940	1.925	1.907	1.698	1.688	1.936	1.909	1.936
Fe2+	2.747	2.608	2.524	2.612	2.565	0.419	0.405	2.544	2.515	2.561
Mn	0.038	0.000	0.000	0.018	0.015	0.051	0.051	0.047	0.051	0.045
Mg	0.303	0.429	0.543	0.472	0.492	0.000	0.000	0.537	0.548	0.495
Ca	0.020	0.034	0.038	0.031	0.046	2.935	2.933	0.025	0.034	0.008
Na	0.052	0.034	0.056	0.047	0.084	0.023	0.031	0.038	0.068	0.040
K	0.000	0.000	0.007	0.000	0.007	0.000	0.000	0.000	0.000	0.000
Total	8.079	8.045	8.085	8.084	8.104	8.145	8.140	8.089	8.102	8.068

Garnet (Recalculated to 12 Oxygens)						
	890-135					
SiO2	37.20	37.20	36.49	36.63	36.60	36.56
TiO2	0.00	0.00	0.00	0.00	0.00	0.35
Al2O3	20.37	20.55	20.77	20.40	20.65	20.72
FeO	37.08	35.45	37.12	37.47	36.73	35.47
MnO	0.50	0.44	0.42	0.40	0.71	0.76
MgO	3.39	4.32	3.35	3.09	3.78	4.33
CaO	0.32	0.44	0.35	0.35	0.13	0.30
Na2O	0.25	0.30	0.40	0.31	0.36	0.25
K2O	0.00	0.00	0.00	0.00	0.00	0.00
Total	99.1	98.7	98.9	98.7	99.0	98.7
Si	3.027	3.017	2.982	3.005	2.985	2.972
Ti	0.000	0.000	0.000	0.000	0.000	0.021
Al	1.954	1.965	2.001	1.973	1.985	1.986
Fe2+	2.523	2.404	2.537	2.571	2.505	2.412
Mn	0.034	0.030	0.029	0.028	0.049	0.052
Mg	0.411	0.522	0.408	0.378	0.459	0.525
Ca	0.028	0.038	0.031	0.031	0.011	0.026
Na	0.039	0.047	0.063	0.049	0.057	0.039
K	0.000	0.000	0.000	0.000	0.000	0.000
Total	8.016	8.024	8.050	8.034	8.051	8.033

Cordierite recalc to 18 O		
	933-54	933-54
SiO2	46.85	47.76
TiO2	0.00	0.00
Al2O3	31.23	31.90
FeO	8.98	9.19
MnO	0.00	0.00
MgO	8.01	8.60
CaO	0.00	0.00
Na2O	0.55	0.49
K2O	0.16	0.08
Total	95.8	98.0
Si	4.990	4.970
Ti	0.000	0.000
Al	3.921	3.914
Fe2+	0.800	0.800
Mn	0.000	0.000
Mg	1.271	1.334
Ca	0.000	0.000
Na	0.114	0.099
K	0.022	0.011
Total	11.117	11.127

Plagioclase recalculated to 8 Oxygens

	933-53	933-54	933-55	933-30	933-45	890-134	
SiO2	66.38	67.02	50.27	66.70	69.39	67.54	65.25
TiO2	0.00	0.00	0.00	0.00	0.00	0.00	0.00
Al2O3	20.90	20.40	24.26	19.93	20.47	18.97	20.84
FeO	0.00	0.00	0.00	0.00	0.18	0.00	0.29
MnO	0.00	0.00	0.00	0.00	0.00	0.00	0.00
MgO	0.00	0.00	0.00	0.00	0.00	0.00	0.00
CaO	1.76	1.14	12.74	0.64	0.66	0.56	1.78
Na2O	10.61	11.37	6.16	11.17	11.70	11.78	10.48
K2O	0.06	0.11	0.34	0.11	0.08	0.29	0.17
Total	99.7	100.0	93.8	98.6	102.5	99.1	98.8
Si	2.919	2.939	2.463	2.961	2.965	2.988	2.904
Ti	0.000	0.000	0.000	0.000	0.000	0.000	0.000
Al	1.083	1.055	1.401	1.043	1.031	0.989	1.093
Fe2+	0.000	0.000	0.000	0.000	0.006	0.000	0.011
Mn	0.000	0.000	0.000	0.000	0.000	0.000	0.000
Mg	0.000	0.000	0.000	0.000	0.000	0.000	0.000
Ca	0.083	0.054	0.669	0.030	0.030	0.027	0.085
Na	0.905	0.967	0.585	0.961	0.969	1.010	0.904
K	0.003	0.006	0.021	0.006	0.004	0.016	0.010
Total	4.993	5.020	5.140	5.002	5.006	5.031	5.007

Muscovite recalc to 11 O

	933-52
SiO2	45.60
TiO2	0.00
Al2O3	35.04
FeO	1.54
MnO	0.00
MgO	0.47
CaO	0.12
Na2O	0.38
K2O	10.79
Total	93.9
Si	3.086
Ti	0.000
Al	2.796
Fe2+	0.087
Mn	0.000
Mg	0.047
Ca	0.009
Na	0.050
K	0.932
Total	7.007

Vesuvianite recalc to 36 O

	933-23	933-23	933-24	933-24
SiO2	37.69	38.35	35.35	35.94
TiO2	0.74	0.54	1.32	1.20
Al2O3	18.21	17.62	15.34	15.59
FeO	5.93	7.85	4.94	5.01
MnO	0.67	0.98	0.23	0.21
MgO	0.00	0.14	1.30	1.16
CaO	34.35	33.67	34.46	34.65
Na2O	0.26	0.29	0.36	0.29
K2O	0.13	0.00	0.00	0.00
Total	98.0	99.4	93.3	94.1
Si	8.964	9.045	8.878	8.938
Ti	0.132	0.096	0.249	0.224
Al	5.106	4.899	4.542	4.571
Fe2+	1.180	1.548	1.038	1.042
Mn	0.135	0.196	0.049	0.044
Mg	0.000	0.049	0.487	0.430
Ca	8.754	8.509	9.273	9.233
Na	0.120	0.133	0.175	0.140
K	0.039	0.000	0.000	0.000
Total	24.430	24.476	24.690	24.622

Scapolite recalc to 24 O

	933-55
SiO2	47.37
TiO2	0.00
Al2O3	22.61
FeO	0.00
MnO	0.00
MgO	0.00
CaO	12.34
Na2O	5.78
K2O	0.41
Total	88.5
Si	7.391
Ti	0.000
Al	4.159
Fe2+	0.000
Mn	0.000
Mg	0.000
Ca	2.063
Na	1.749
K	0.082
Total	15.444

Diopside recalculated to 6 Oxygens

	933-23		933-24		933-55
SiO2	48.67	48.77	50.92	51.48	52.87
TiO2	0.00	0.00	0.00	0.00	0.00
Al2O3	0.36	0.44	2.69	0.16	1.10
FeO	23.61	24.61	17.49	12.98	17.10
MnO	1.22	1.18	1.02	1.55	0.67
MgO	2.07	2.01	10.84	8.94	12.18
CaO	22.42	22.73	13.34	24.35	12.25
Na2O	0.21	0.42	0.23	0.20	0.30
K2O	0.00	0.00	0.09	0.00	0.07
Total	98.6	100.2	96.6	99.7	96.5
Si	1.999	1.982	1.999	1.993	2.058
Ti	0.000	0.000	0.000	0.000	0.000
Al	0.017	0.021	0.125	0.007	0.050
Fe2+	0.811	0.836	0.574	0.420	0.557
Mn	0.042	0.041	0.034	0.051	0.022
Mg	0.127	0.122	0.634	0.516	0.706
Ca	0.987	0.990	0.561	1.010	0.511
Na	0.017	0.033	0.018	0.015	0.023
K	0.000	0.000	0.005	0.000	0.003
Total	4.000	4.024	3.950	4.011	3.930

Epidote recalculated to 12.5 O

	933-55		933-24
SiO2	36.81	29.37	37.41
TiO2	0.00	0.00	0.00
Al2O3	24.46	16.55	25.62
FeO	7.47	10.44	7.41
MnO	0.00	0.00	0.14
MgO	0.00	0.00	0.12
CaO	22.09	15.12	23.20
Na2O	0.22	0.00	0.31
K2O	0.00	0.00	0.00
Total	91.1	71.5	94.2
Si	3.130	3.251	3.081
Ti	0.000	0.000	0.000
Al	2.452	2.159	2.487
Fe2+	0.531	0.966	0.510
Mn	0.000	0.000	0.010
Mg	0.000	0.000	0.015
Ca	2.013	1.793	2.047
Na	0.036	0.000	0.050
K	0.000	0.000	0.000
Total	8.162	8.170	8.200

Chlorite recalc to 16 O

	933-52	890-134	
SiO2	22.13	24.77	23.98
TiO2	0.00	0.00	0.10
Al2O3	21.52	18.12	19.18
FeO	31.46	27.87	28.46
MnO	0.00	0.00	0.17
MgO	10.29	13.49	12.92
CaO	0.00	0.09	0.07
Na2O	0.00	0.21	0.35
K2O	0.00	0.11	0.00
Total	85.4	84.7	85.2
Si	2.856	3.161	3.054
Ti	0.000	0.000	0.010
Al	3.275	2.726	2.879
Fe2+	3.396	2.975	3.031
Mn	0.000	0.000	0.018
Mg	1.979	2.566	2.452
Ca	0.000	0.012	0.010
Na	0.000	0.052	0.086
K	0.000	0.018	0.000
Total	11.506	11.510	11.540

Actinolite recalc to 23 O

	933-24	933-24
SiO2	52.11	51.70
TiO2	0.00	0.00
Al2O3	0.44	2.47
FeO	18.42	17.24
MnO	1.76	1.05
MgO	10.43	11.41
CaO	12.34	12.25
Na2O	0.27	0.45
K2O	0.00	0.16
Total	95.8	96.7
Si	7.941	7.734
Ti	0.000	0.000
Al	0.079	0.436
Fe2+	2.348	2.157
Mn	0.227	0.133
Mg	2.369	2.544
Ca	2.015	1.964
Na	0.080	0.131
K	0.000	0.031
Total	15.059	15.128

APPENDIX C: Sample localities with respect to the marble marker bed.

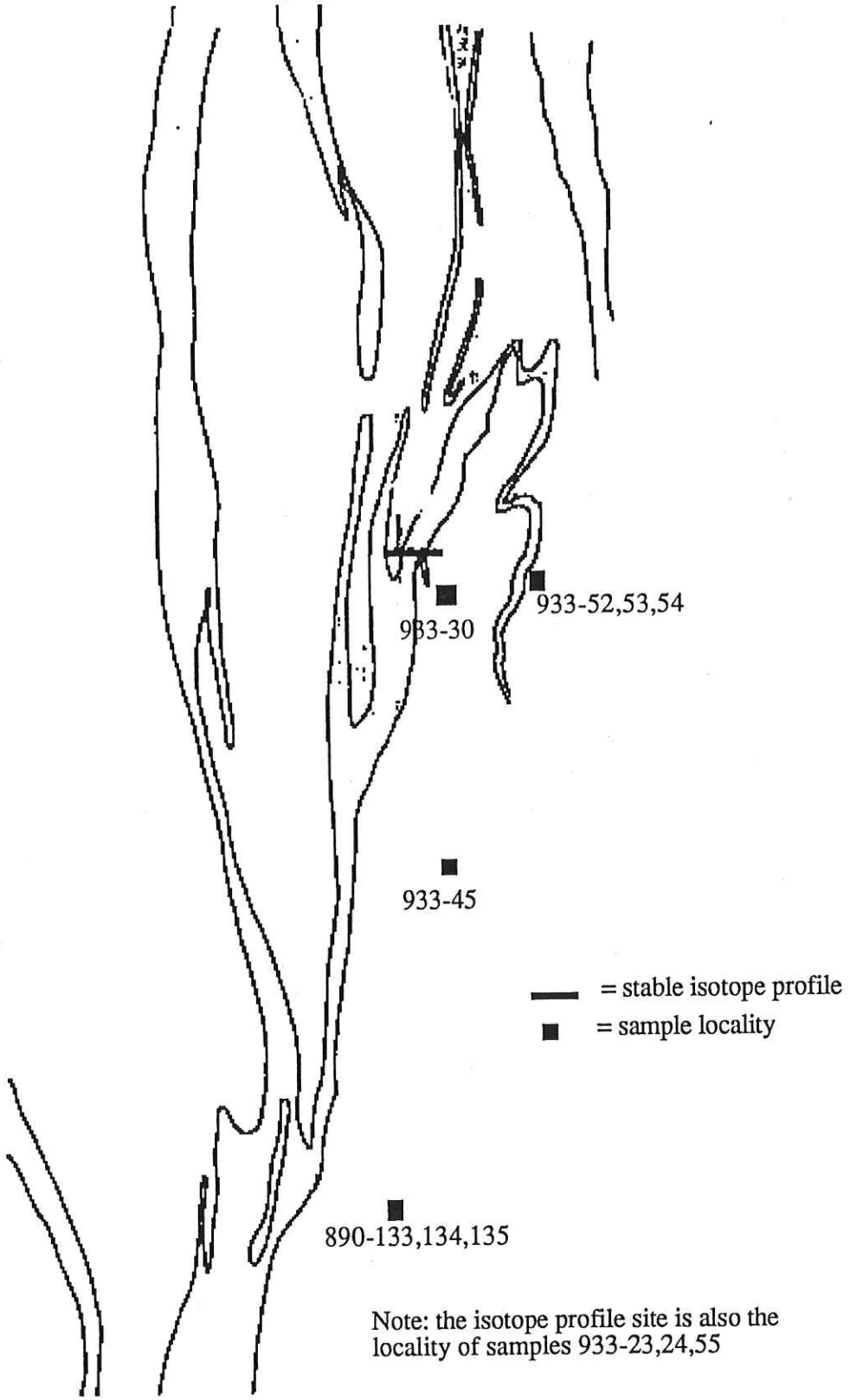

APPENDIX D; Mathematical Background to the Fluid Flow Treatment

The variation in concentration of a chemical tracer in a fluid with distance, z, and time, t, is described by the equation;

$$\left(\frac{\rho_s K_c}{\rho_f} + \phi\right)\frac{dC_f}{dt} + \phi\,\omega_o\frac{dC_f}{dz} = D_{eff}\frac{d^2C_f}{dz^2}$$

where ρ is the density, subscripts s and f refer to solid and fluid respectively, K_c is the distribution coefficient between solid and fluid, ϕ is the porosity, ω_o is the fluid velocity, D_{eff} is the effective diffusivity of the two phase material.

Transformation to dimensionless variables reduces this equation to

$$\frac{dC'_f}{dt} + Pe\frac{dC'}{dz'} = \frac{d^2C'}{dz'^2}$$

where; $Pe = \dfrac{\phi\,\omega_o\,h}{D_{eff}} = \dfrac{W_o\,h}{D_{eff}}$, W_o = fluid flux

Solution of this equation for pinned boundary conditions
ie. C' = 0 at z' =o and 1 for all times
and the initial condition that C' = 1 between z' = 0 and 1, gives;

$$C' = 2\,\pi\,e^{(Pe\,z'/2)}\,\text{sigma}\,\frac{n}{(Pe/2)^2 + n^2\,p^2}\,((-1)^n e^{Pe/2} - 1)$$
$$\exp[-((Pe/2)^2 + n^2\,p^2)\,t']\,\sin(n\,\pi\,z')$$

which can be solved for various values of Pe to give curves of the form shown in Figure 7 in the text.

APPENDIX E; Mathematical Background to Heat Flow relevant to the numerical modelling discussed in the text.

The pascal program, "Crank_heat " (included after this appendix) uses an implicit, Crank-Nicholson, finite difference approximation to the one dimensional heat equation to model the thermal evolution of rocks surrounding an intrusive sill.

In a purely conductive regime the one-dimensional heat transfer equation is;

$$\frac{d^2T}{dx^2} = \frac{1}{\kappa}\frac{dT}{dt} + \frac{\upsilon}{\kappa}\frac{dT}{dx} - \frac{A(x,t)}{K}$$

Where T is temperature, κ is thermal diffusivity, u is the vertical velocity of the rocks with respect to the surface, K is the thermal conductivity, u is the vertical velocity of the rocks with respect to the surface and K is the thermal conductivity.
Intrusion of magma may be simulated by imposing the initial condition of a realistic magmatic temperature eg.750°C, over some depth corresponding to the depth of the modelled sill. For simplicity the effects of erosion have been ignored so the second term on the right hand side of the heat equation drops out.

Latent heat of fusion, L, released as intrusive magmas crystallise, is accounted for by modifying the heat capacity of the magma, C_p, to C' where;

$$C' = C_p + \frac{L}{T_l - T_s}$$

Tl is the liquidus temperature, Ts is the solidus temperature.
The thermal diffusivity used in the heat equation is then given by

$$\kappa(T) = \frac{K}{\rho C'}$$

Jaeger (1964) has shown that poorly understood details about the mode of solidification of a magmatic sill have little effect on temperature variations at distances greater than a quarter sill thickness from the intrusive contact and hence are ignored here.

The Crank-Nicholson scheme approximates the derivatives required as follows;

$$\left(\frac{d^2T}{dx^2}\right)_{i,j+1/2} = \frac{1}{2}\left\{\frac{(T_{i+1,j+1} - 2T_{i,j+1} + T_{i-1,j+1})}{h^2} + \frac{(T_{i+1,j} - 2T_{i,j} + T_{i-1,j})}{h^2}\right\}$$

and

$$\frac{dT}{dt} = \frac{(T_{i,j+1} - T_{i,j})}{k}$$

where i = space iteration, j = time iteration, h = space step, k = time step

```
program Crank_heat;

{version 1.0}
{Geoff Fraser and Mike Sandiford}
{28.8.90 - .....}
{with latent heat modifications 30.8.90}

 const

              {*******   grid   steup******}

   n = 101;
   del_t = 8e8;                {time steping interval}
   max_timesteps = 100;          {maximum timesteps}
   drawstep = 10;                  {number of timesteps between drawing}

            {*******physical   constants******}

   kappa = 1e-6;                   {thermal  diffusivity}
   Lat_heat = -5.5e6;                      {latent heat of fusion : Kj kg-1}
   Cp = 1.1e3;                     {heat capacity : Kj kg-1 K}
   del_z = 1000;                   {initial vertical spacing between grid points}
   T_base = 1280;                  {temperature at base of grid}
   T_surface = 0;                  {temperature at top of grid}
   Tl = 1000;                      {liquidus : C}
   Ts = 700;                       {solidus : C}
   ro = 2800;                      {density : kg m-3}

 var
   L_H_term,                       {term used in latent heat calculations}
   m_temp,                         {initial temperature of magma}
   R, R_L,                         {fourier number}
   A, B, C,                        {Crank-Nicholson variables}
   xscale,                         {drawing routine}
   yscale                          {drawing routine}
   : real;

   Z,                              {space grid}
   T,                              {temperature grid}
   preT                            {temperatures at previous time step}
   : array[1..n] of real;

   intr_top,                       {depth to top of intrusion}
   intr_bot,                       {depth to base of intrusion}
   counter,                        {counts number of timesteps}

   i: integer;

{==================================}

  procedure initial_conditions;


    {====================}

   procedure input;
```

```
  begin
    writeln('magmatic temperature (°C): ');
    readln(m_temp);
    writeln('node at top of intrusion (km) : ');
    readln(intr_top);
    writeln('node at bottom of  intrusion (km) : ');
    readln(intr_bot);
  end;

    {====================}

  procedure depth_array;

    var
      i: integer;

  begin
    Z[1] := 0;
    for i := 2 to n do
      begin
        Z[i] := Z[i - 1] + del_Z;
      end;
  end;


  {====================}

{**********warning : assumes initial linear geotherm**********}

  procedure initial_temperatures;

    var
      del_T_i                  {initial temperature step}
      : real;
      i: integer;

  begin

    del_T_i := (T_base - T_surface) / (Z[n] - Z[1]) * del_Z;
    T[1] := T_surface;
    for i := 2 to n do
      begin
        T[i] := T[i - 1] + del_T_i;
      end;
    for i := intr_top to intr_bot do
      begin
        T[i] := m_temp
      end;
  end;

    {====================}

  begin
    input;
    depth_array;
    initial_temperatures;
    R := (del_t * kappa) / sqr(del_z);
    writeln(' R == ', R : 4 : 2);
```

```
  L_H_term := 1 - ((lat_heat * ro) / (Cp * ro * (Tl - Ts)));
  R_L := R / L_H_term;
 end;

{==================================}

 procedure main_calculations;

  var
   i: integer;
   E: array[1..n] of real;

  {====================}

  procedure tridiagonal;

  {Tridiagonal algorithm from Press et al. }
  {- Numerical recipes -}

   var
    bet: real;
    gam: array[1..n] of real;
    i: integer;

  begin

   E[2] := E[2] - A * T[1];
   E[n - 1] := E[n - 1] - C * T[n];

   bet := B;
   T[2] := E[2] / bet;
   for i := 3 to (n - 1) do
    begin
     gam[i] := C / bet;
     bet := b - a * gam[i];
     T[i] := (E[i] - a * T[i - 1]) / bet;
    end;
   for i := (n - 2) downto 2 do
    T[i] := T[i] - gam[i + 1] * T[i + 1];

  end;

   {====================}

  procedure crank_nicholson;


   var
    i: integer;

  begin
   for i := 2 to n - 1 do
    begin
     If (preT[i] > Ts) and (preT[i] < Tl) and (i <= intr_bot) and (i >= intr_top) then
      begin
       E[i] := R_L * preT[i + 1] + (2 - 2 * R_L) * preT[i] + R_L * preT[i - 1];

      end
```

```
        else
          begin
            E[i] := R * preT[i + 1] + (2 - 2 * R) * preT[i] + R * preT[i - 1];
          end;
      end;
  end;



    {====================}

  begin
    if counter = 1 then
      begin
        R := (del_t * kappa) / sqr(del_z);
        A := -R;
        C := -R;

      end;
    B := 2 + 2 * R;
    crank_nicholson;
    tridiagonal;
  end;

{==================================}

  procedure output;

    const
      xor = 30;
      yor = 30;
      xmax = 330;
      ymax = 330;
    var
      arect: rect;
      i: integer;

      {====================}

    procedure initialise_drawing;

    begin
      xscale := (xmax - xor) / (T_base - T_surface);
      yscale := (ymax - yor) / (Z[n] - Z[1]);
      with arect do
        begin
          top := 10;
          left := 10;
          bottom := 400;
          right := 400;
        end;
      setdrawingrect(arect);
      showdrawing;

      drawline(xor, yor, xor, ymax);
      drawline(xor, yor, xmax, yor);
```

```
  end;

    {====================}

 begin
  if counter = 1 then
    begin
      initialise_drawing
    end;
  for i := 2 to n do
    begin
      drawline(xor + round(xscale * T[i - 1]), yor + round(yscale * z[i - 1]), xor + round(xscale *
       T[i]), yor + round(yscale * z[i]))
    end;
 end;

{==================================}

begin

 initial_conditions;
 counter := 1;
 output;

 repeat
  for i := 1 to n do
    begin
      PreT[i] := T[i]
    end;
   main_calculations;
   if round(counter / drawstep) = (counter / drawstep) then
    begin
      output
    end;
   counter := counter + 1;
 until counter > max_timesteps;

end.
```